STUDY OF THE STRUCTURAL, MAGNETIC AND ELECTRICAL PROPERTIES OF NICKEL - CADMIUM FERRITES.

BY

SUMAN KUMAR NATH
ROLL NO. 0 1 5 5 5 0 1
SESSION: 2001 – 2002

A THESIS SUBMITTED TO THE DEPARTMENT OF PHYSICS
KHULNA UNIVERSITY OF ENGINEERING & TECHNOLOGY
IN PARTIAL FULFILLMENT OF THE REQUIREMENT FOR THE DEGREE OF
MASTER OF PHILOSOPHY

DEPARTMENT OF PHYSICS
KHULNA UNIVERSITY OF ENGINEERING & TECHNOLOGY
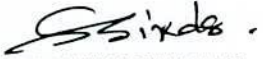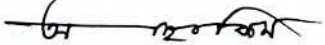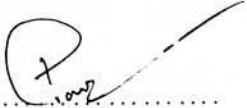KHULNA-920300, BANGLADESH

JULY, 2006

KHULNA UNIVERSITY OF ENGINEERING & TECHNOLOGY
DEPARTMENT OF PHYSICS
CERTIFICATION OF THESIS WORK

A THESIS ON

Study of the Structural, Magnetic and Electrical properties of Nickel-Cadmium ferrites

By
SUMAN KUMAR NATH

has been accepted as satisfactory in partial fulfillment for the degree of Master of Philosophy in Physics and certified that the student has demonstrated a satisfactory knowledge on the field covered by this thesis in an oral examination held on 29 July, 2006.

1. Professor Dr. Shibendra Shekher Sikder
    Department of Physics
    Khulna University of Engineering & Technology

    Chairman & Supervisor

2. Head
    Department of Physics
    Khulna University of Engineering & Technology

    Member

3. Dr. A. K. M. Abdul Hakim
    Chief Engineer
    Materials Science Division
    Atomic Energy Centre, Dhaka

    Member & Joint Supervisor

4. Professor Dr. Md. Mahbub Alam
    Department of Physics
    Khulna University of Engineering & Technology

    Member

5. Dr. Md. Feroz Alam Khan
    Associate Professor
    Department of Physics
    Bangladesh University of Engineering & Technology
    Dhaka-1000

    Member (External)

CERTIFICATE

It is to certify that this thesis which the candidate has presented for M. Phil degree has been done by the candidate himself and does not contain any material extracted from elsewhere or from a work published by any body else. The work of this thesis has not been presented for another degree or diploma in any other University or Institute. No other person's work has been used without due acknowledgement.

_____
Supervisor

_____
Candidate

TO

The parents, specially
my Beloved Mother
who teaches me without telling.

Acknowledgement

ABSTRACT

This thesis describes the experimental investigation of the structural, magnetic and electrical properties of $Ni_{1-x}Cd_xFe_2O_4$ ferrites for $0.0 \leq x \leq 0.8$, prepared by conventional double sintering ceramic method. The characterization of the samples has been performed by X-ray diffraction. Magnetic properties have been measured as a function of field, temperature and frequency, using vibrating sample magnetometer, SQUID magnetometer and Impedance Analyzer. X-ray diffraction results confirmed the single-phase spinel structures of all the studied ferrite samples. The lattice parameter increases linearly with increasing Cd concentration obeying Vegard's law. This is attributed to the replacement of smaller Fe^{3+} ions (0.64Å) from A-sites to B-sites by larger Cd^{2+} ions (0.97 Å). The bulk density of the samples increases monotonically with increasing Cd content signifying that Cd has a pronounced effect on the densification of the ferrites. Curie temperature decreases linearly with increasing Cd content which has been explained due to the weakening of A-B exchange interaction. Saturation magnetization at 20K increases with Cd content up to $x = 0.5$ and decreases thereafter. Neel's two sublattice collinear model is applied for the initial rise of the magnetization up to $x \leq 0.5$ and beyond that three sublattice non-collinear model proposed by Yafet-Kittel are predominant. This suggests the existence of canted spin structure in the ferrite system with higher content of Cd. The sample with $x = 0.8$ shows anomalous temperature dependent magnetic ordering on applied magnetic field. Low field (5 Oe) magnetization shows antiferromagnetic ordering at 39K while the ferromagnetic ordering with $T_c = 172K$ is dominant with the application of high field (1 T). This implies that the magnetic ordering in this sample is dependent on magnetic field. Permeability increases with increasing Cd concentration as well as increasing sintering temperature for all the studied samples. The increase of permeability is ascribed to the increase of density and grain size. For the sample with $x=0.6$, the permeability decreases with increasing sintering temperature in spite of high density which may be attributed to the intragranular porosity that inhibits easy domain wall mobility resulting in a decrease of permeability. Room temperature DC resistivity decreases with Cd content and sintering temperature.

CONTENTS

CHAPTER - I

Introduction

1.1 Introduction

Ferrites are commercially important magnetic materials. Ranging from the very ordinary radio sets to the complicated and exhaustive hardware involved in computers, ferrites have found their way to prove their importance. There are soft and hard magnetic ferrites. Both of these ferrites have enormous practical applications. Soft ferrites have been extensively used for many kinds of magnetic devices such as transformers, inductors, magnetic heads, in resonance circuit for high frequency (ranging from 10^3 to 10^{11}Hz) because of their electrical resistivity higher than those of the soft magnetic alloys (ranges from 10^3 to 10^{11} Ω-cm which is up to 15 order of magnitude higher than that of metals like iron), low eddy current losses, high initial permeability, high saturation induction, low histeresis loss and reduced physical size. Due to these reasons extensive research activities has been carried out during the past 50 years to enhance their efficiency from the application point of view to various technical devices.

Soft ferrites belong to cubic spinel structure while hard ferrites to magnetoplumbite hexagonal structure. In these present work soft magnetic ferrites of cubic spinel structure with a composition of Ni-Cd has been carried out.

A large number of oxides with a metal-oxygen ratio of 0.75 as composition are known to crystallize into the spinel structure, which is called after the mineral spinel $MgAl_2O_4$. Among these oxides, magnetite Fe_3O_4 is an important compound, from which the spinel ferrites can be derived by partial substitution of the iron ions by other cations. Between most of the spinel oxides solid solutions can be formed, which means that a great variety of spinel oxides is possible. If we restrict ourselves to the spinel ferrites, the general chemical formula of these materials is $M'Fe^{3+}_{2-x}M''_xO_4$, in which Me' represents a divalent cation, or a combination of cations with an average valency of two, and M'' a trivalent cation or a combination of cations with an average valency of three. The composition parameter can range between zero and two, but it is obvious that if x is close to two, these oxides cannot be considered anymore as ferrites.

2

The so-called simple spinel ferrites are now those ferrites in which x = 0 and the divalent metal ion is Mg or Cd or one of the divalent transition metal elements Mn, Fe, Co, Ni, Cu and Zn. The solid solutions between the simple ferrites are called the mixed ferrites. Although the spinel ferrite materials are widely used for so many years in eletro-technical equipment, much research and development in this field is still in progress, from the basic as well as from the application point of view. Although there have been no novel developments in ferrite materials and components, world production of ferrites is still increasing and the development problems connected with these technically important materials are yet to be solved. As magnetic materials, ferrites are still the best in high frequency and very high frequency circuits and they cannot be replaced by other magnetic elements, since they are relatively inexpensive and easy to fabricate [1].

A wealth of information regarding the development of soft ferrites as regards to their magnetic, electrical, optical and dielectric properties are available [2-4].

Cubic spinel ferrite, has two sub-lattices, tetrahedral (A site) and octahedral (B site) in AB_2O_4 crystal structure. The important structural, electrical and magnetic properties of spinels, responsible for their application in various fields, are found to depend on the distribution of cations among the sites [5].

Therefore the estimation of the cation distribution turns out to be important. Various cations can be placed in A site and B site to tune its magnetic properties. Depending on A site and B site cations it can exhibit various magnetic structures [6].

The magnetic properties of the spinel ferrites are governed by the type of magnetic ions residing on the A- and B-sites and the relative strengths of the inter-(J_{AB}) and intra-sublattice (J_{AA}, J_{BB}) exchange interactions. When the cations of A and B sites are totally magnetic, the inter-exchange interactions J_{AB} are much stronger than the A-A and B-B intra-sublattice interactions; the spins have a collinear structure in which moments on the A-sites are anti-parallel to the moments on the B-sites. The advantage of the mixed spinel is that all interactions are well defined near-neighbour anti-ferromagnetic, with $|J_{AB}| \gg |J_{BB}| \gg |J_{AA}|$.

When one of the intra-sublattice interactions becomes comparable with the inter-sublattice interaction it leads to a non-collinear spin structure [7].

Thus, J_{AB} renders the undiluted spinel ferrimagnetic with all A-site moments oriented anti-parallel to all B-site moments, but with BB and AA bonds remaining unsatisfied. On dilution, frustration of certain moments should occur leading to collapse of the co-linearity of the ferrimagnetic phase and the effective moments are created within the ferrimagnetic structure by local canting around the magnetic imperfections. It is well known that when ferrites are sufficiently diluted with non-magnetic atoms they can show a wide spectrum of magnetic order ranging from ferrimagnetism, anti-ferromagnetism, local canted spin to semi-spin glass, spin glass and paramagnetic behaviour. Nickel ferrite belongs to the partially inverse spinel and it can be considered as a collinear ferrimagnet while Cadmium ferrite is a normal spinel.It is known that Zn^{2+} and Cd^{2+} ions have similar effects; both of them are non-magnetic and prefer to occupy the tetrahedral sites only [4]. Therefore it is of interest in the present thesis to investigate the magnetic, structural and electrical properties of Ni-Cd ferrite.

1.2 Objective of the Present Work

$Ni_{1-x}Zn_xFe_2O_4$ system is a established well known ferrite materials to be used in various electromagnetic devices due to their high resistivity, high permeability and comparatively low magnetic losses. Zn and Cd are both non-magnetic and both Zn-ferrite and Cd-ferrite are normal spinel. Therefore it is interesting to substitute Cd with Ni to understand it's effect on the magnetic , electrical and structural properties , which have hitherto not been studied in much detail. Moreover this is to note that the ionic radii of Cd are larger than Zn. So substitution of Cd with Ni is expected to show some interesting magnetic, electrical and structural properties.

4

The main objectives of the present research are as follows:

- Preparation of various $Ni_{1-x}Cd_xFe_2O_4$ (for x = 0.0 to 0.6 in step of 0.1 and 0.8) samples by standard ceramic double sintering method.
- Determination of phases, structure, density and porosity of the samples.
- Determination of ferrimagnetic to paramagnetic transition temperature, T_c from the measurement of temperature dependence of initial permeability.
- Evaluation of initial permeability as a function of frequency (1kHz-13MHz) for samples having various microstructures (e.g. grain size) as affected by varying sintering temperatures.
- Measurement of saturation magnetization and it's dependence on Cd content.
- From the detail studies of the magnetic properties on sintering temperature (T_s), an optimum T_s would be determined that corresponding to the composition exhibiting optimum soft magnetic properties.

1.3 Summary of the Thesis

The format of the thesis is as follows:

Chapter - I of the thesis deals with a brief overview of materials, importance and objectives of the present work.

Chapter - II gives the theoretical background and the crystal structure of the spinel ferrites.

Chapter - III gives the details of the sample preparation.

Chapter - IV describes the experimental part and descriptions of different measurement techniques that have been used in this research work.

Chapter -V is devoted to the results of various investigations of the study and their interpretation based on the existing theories and models.

The conclusions drawn from the overall experimental results and discussion are presented in

Chapter - VI

Some specific experimental data, symbols and units are given in **Appendix** .

References :

[1] J Kulikowski- J Magn. Mat. **41**(1984) 56-62.

[2] Alex Goldman-Handbook of Modern Ferromagnetic Materials, Kluwer Academic Publishers, London.

[3] V.A.M. Bravers – Progress in Spinel Ferrite Research in Handbook of Magnetic Materials, Editted by K.H.J. Buchow, North Holland Publishing Inc. **8** (1995)191-324.

[4] J. Smit and H. P. J. Wijn-FERRITES John Wiley & Sons Publishers, (1959).

[5] A. Meenakshisundaram, N. Gunasekaran, V. Srinivasan, Phys. Status Solidi (a) **69** (1982) KIS.

[6] A.K.M. Akther Hossain, M. Seki, T. Kawai, H. Tabata, J. Appl. Phys. **96 (2)** (2004)1273.

[7] Y. Yafet and C. Kittel, Phys. Rev. **87** (1952)290.

CHAPTER - II

Theoretical Background

2.1 Introduction to Magnetic Ordering

The onset of magnetic order in solids has two basic requirements:

(i)   individual atoms should have magnetic moments (spins),

(ii)   exchange interactions should exist that couple them together[1].

Magnetic moments originate in solids as a consequence of overlapping of the electronic wave functions with those of neighbouring atoms. This condition is best fulfilled by some transition metals and rare-earths. The exchange interactions depend sensitively upon the interatomic distance and the nature of the chemical bonds, particularly of nearest neighbour atoms. When the positive exchange dominates, which corresponds to parallel coupling of neighbouring atomic moments (spins), the magnetic system becomes ferromagnetic below a certain temperature T_c called the Curie temperature. The common spin directions are determined by the minimum of magneto-crystalline anisotropy energy of the crystal. Therefore, ferromagnetic substances are characterized by spontaneous magnetization. But a ferromagnetic material in the demagnetized state displays no net magnetization in zero field because in the demagnetized state a ferromagnet of macroscopic size is divided into a number of small regions called domains, spontaneously magnetized to saturation value and the directions of these spontaneous magnetization of the various domains are such that the net magnetization of the specimen is zero. The existence of domains is a consequence of energy minimization. The size and formation of these domains is in a complicated manner dependent on the shape of the specimen as well as its magnetic and thermal history. When negative exchange dominates, adjacent atomic moments (spins) align anti-parallel to each other, and the substance is said to be anti-ferromagnetic below a characteristic temperature, T_N, called the Neel temperature. In the simplest case, the lattice of an antiferromagnet is divided into two sub lattices with the magnetic moments of these in anti-parallel alignment. This results in zero net magnetization. A special case of anti-ferromagnetism is ferrimagnetism.

8

In ferrimagnetism there are also two sub-lattices with magnetic moments in opposite directions, but the magnetization of the sub-lattices are of unequal strength resulting in a non-zero magnetization and therefore has net spontaneous magnetization. At the macroscopic level of domain structures, ferromagnetic and ferrimagnetic materials are therefore similar. The Curie and Neel temperatures characterize a phase transition between the magnetically ordered and disordered (paramagnetic) states. From these simple cases of magnetic ordering, various types of magnetic order exist, particularly in metallic substances. Because of long range order and oscillatory nature of the exchange interaction, mediated by the conduction electrons, structures like helical, conical and modulated patterns might occur. Examples of different types of magnetic order are shown in Fig. -2.1 [2].
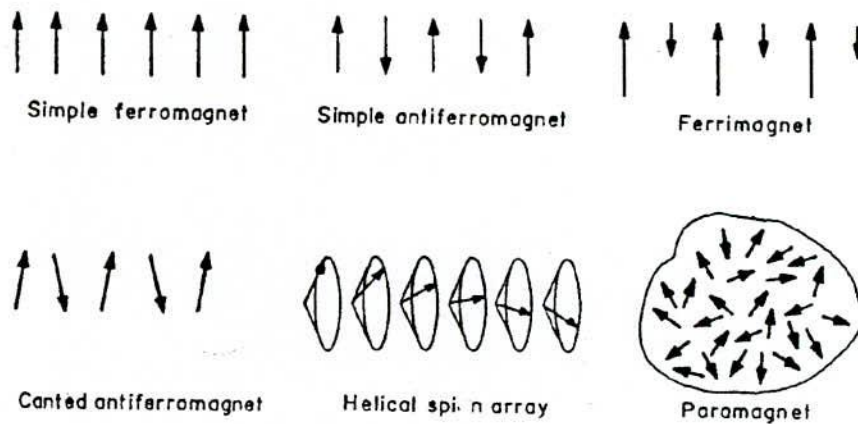
Figure 2.1: Examples of different types of magnetic order using a linear array of localized moments, including paramagnet.

2.2 Theory of Ferrimagnetism

Ferrimagnetic substances exhibit a substantial spontaneous magnetization at room temperature, just like ferromagnetics, and this fact alone makes them industrially important. Again like ferromagnetics, they consist of self-saturated domains, and they exhibit the phenomena of magnetic saturation and hysteresis. Their spontaneous magnetization disappears above a certain critical temperature T_c also called the Curie temperature, and then they become paramagnetic. Ferrimagnetics were not recognized as forming a distinct magnetic class until 1948. In a classic paper published in 1948, Neel provided the theoretical key to an understanding of ferrimagnetism in general and ferrites in particular.

The word ferrimagnetism was coined by Neel to describe the properties of those substances which below a certain temperature exhibit spontaneous magnetization arising from a non-parallel alignment of atomic magnetic moments. In his original paper Neel envisaged a partitioning of the moments into two sub-lattices, which because of their mutual interaction are aligned antiparallel to each other, thus producing a total magnetic moment equal to the difference between their individual magnitudes.

Almost all known ferrimagnetic compounds have rather complex structures, with at least two crystallographically inequivalent sites for the magnetic ions to provide a basis for the sub-lattices. The temperature at which long-range order sets in, now generally known as the Neel point T_N, is determined largely by the strength of the interaction between nearest neighbours, though under special conditions of symmetry other factors may also be important [3].The difference mentioned above, can arise in several ways, and some of these are shown diagrammatically in Fig.2.2 [4]. Fig. 2.2(a) shows the case in which there are different numbers of similar magnetic moments in the sub-lattices. In some respects this arrangement superficially resembles that of a normal antiferromagnetic substance with unequal partitioning of the sub-lattices, but many of the properties of such a substance are similar to those of a ferromagnet with a reduced number of magnetic

moments. Fig. 2.2(b) shows the case of equal numbers of dissimilar moments. The dissimilarity can arise either because the magnetic ions are chemically different, or because a different local environment leads to different effective magnetic moments in ions having the same spin. So far only the first of these possibilities has been observed. A third type of arrangement is shown in Fig. 2.2(c). This is the case originally considered by Neel and it represents a very large number of substances, including most of the ferrites. In this arrangement one sub-lattice contains two different types of magnetic moment, one of which also occurs in equal numbers on the second sub-lattice, so that the net effect is that of just the one type of moment. An extension of this case arises when the second sub-lattice also contains two types of moments, as shown in Fig. 2.2(d). An extension of the Neel theory has been given by Yafet and Kittel (1952) [5], who pointed out that if there are strong interactions between the ions within a given sub-lattice, in addition to the interaction between the sub-lattices, then a triangular arrangement ay be favoured such as shown in Fig. 2.2(e) which will have a lower energy than the uniaxial Neel type arrangements. Obviously such situations can be extended to a large number of variants, involving various three-dimensional multi-spin-axis arrangements.

An alternative type of multi-spin-axis arrangement, which does not seem to have been considered before, arises when there are strong local anisotropy forces tending to hold each spin in a particular direction relative to the crystal sub-lattice. Consider, for example, the simple case of a cubic crystal in which one sub-lattice consists of three types of moment, each of which is bound by some anisotropy forces to one of the three cube axes. Interaction with a second sub-lattice, which we may for simplicity assume to be free, then produces a compromise arrangement such as shown in Fig. 2.2(f). So far there is no direct experimental evidence for such an arrangement, but it seems very likely that some ferrimagnetic rare earth compounds have this type of arrangement.

11
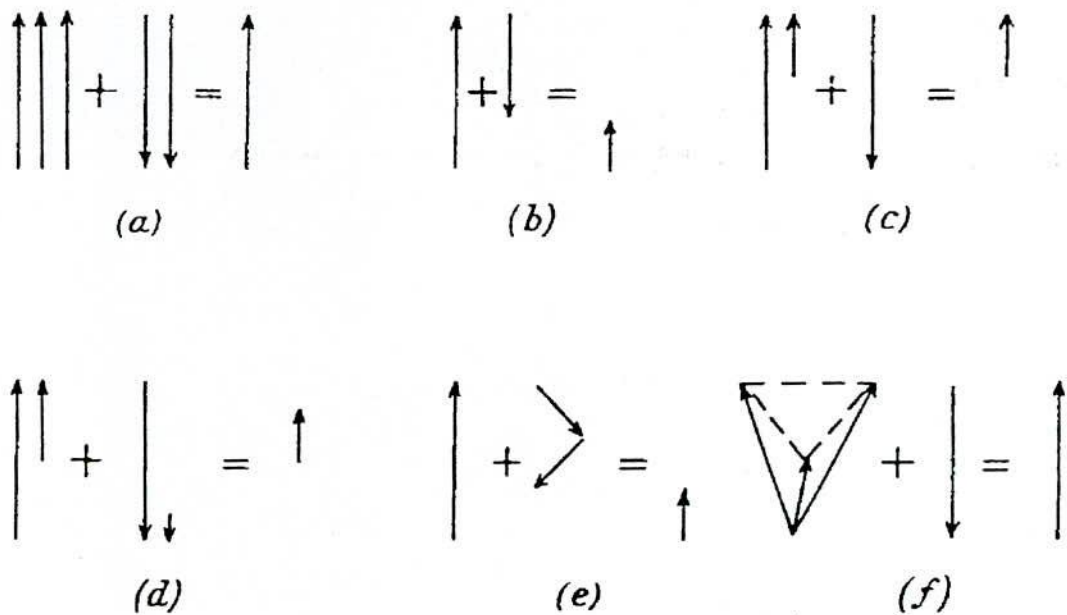
Figure-2.2: Illustration of six simple sub-lattice arrangements which can give rise to a spontaneous ferromagnetic moment.

In general there is nothing to limit the number of sub-lattices and their direction of alignment, and it is important to realize that the simple arrangements we have discussed are only a first approximation in most real crystals. However, for the explanation of many phenomena the simple Neel theory is often quite adequate.

Several facts led Neel to envisage a distinct form of magnetic structure for the ferrites. Crystallographic studies have provided the clue that the cations in a ferrite crystal occupy two crystallographically different kinds of position called A- sites and B-sites. Neel made the basic assumption that the exchange interaction between these two sites is negative, meaning that the spin orientation is opposite to each other. This thing also happens in antiferromagnetism. The difference is that, in case of ferrimagnetism magnitudes of the A

and B sublattice magnetizations are not equal and a net spontaneous magnetization results.

The exchange interaction acting in ferrites is of a different kind. As pointed out by Neel, the cations are mutually separated by bigger anions (oxygen ions) which practically exclude a direct contact between the cation orbital, making any direct exchange at least very weak. Instead, we encounter Supper Exchange i.e. indirect exchange via oxygen p orbital that may be strong enough to order the magnetic moments. The strength of this interaction depends on the degree of orbital overlap of oxygen p orbital and transition metal d orbital. The interaction decreases as the metal ions move apart and the angle between them decreases from 180^0 to 90^0. In Neel's theory, the interaction are taken as effective inter and intra-sublattice interactions A-A, B-B and A-B. The type of magnetic order depends on their relative strength. The theory of super exchange and semi-empirical rules provided by Goodenough [6] yields some predictions concerning the sign and strength of this interaction. It is found that A-A interaction is weak compared to B-B interaction. But angle between B-B interaction is 90^0 thus making it weak compared to A-B interaction where angle is 125^0. Thus antiparallel spin alignment takes place in two sublattices. The interaction energy density may be written as

$$U = -2\,J\,S_i - S_j \qquad (2.1)$$

The exchange integral, J in equation (2.1) is positive, we achieve ferromagnetism. A negative J may give rise to anti-ferromagnetism or ferri-magnetism. The mean exchange fields acting on A and B sites may be written as

$$B_A = \lambda M_A - \mu M_B$$
$$B_B = \mu M_A - v\,M_B \qquad (2.2)$$

All constants λ, μ, v are taken to be positive. The minus sign then corresponds to an anti-parallel interaction. The interaction energy density is

$$U = -1/2\,(B_A\,.M_A + B_B\,.\,M_B)$$
$$= 1/2\,\lambda\,M_A{}^2 + \mu M_A M + 1/2\,VM_B{}^2 \qquad (2.3)$$

This is lower when M_A is anti-parallel to M_B than when M_A is parallel to M_B. The energy of anti-parallel alignment should be compared with zero, because a possible solution is $M_A = M_B = 0$. Thus when

$$\mu M_A M_B > \tfrac{1}{2}(\lambda M_A{}^2 + v M_B{}^2)$$

the ground state will have M_A directed opposite to M_B. Under certain conditions there may be non-collinear spin arrays of still lower energy.

The susceptibility of ferrimagnets is readily formulated if we assign separate Curie constants C_A and C_B to the two sublattices. Neglecting intra sublattice interaction we have ferrimagnets:

Sub lattice A	Sub lattice B	
$B_A = -\mu M$	$B_B = -\mu M_A$	(2.4)
$M_A T = C_A (B_a - \mu M_B)$	$M_B T = C_B (B_a - \mu M_A)$	

Here B_A is applied field. These equations have a non zero solution for M_A and M_B in zero applied field if

$$\begin{vmatrix} T & \mu C_A \\ \mu C_B & T \end{vmatrix} = 0 \qquad (2.5)$$

from which the ferrimagnetic Curie temperature $T = \theta_F$ is given by

$$\theta_F = \mu (C_A C_B)^{1/2} \qquad (2.6)$$

we solve eqn. (2.4) for M_A and M_B to obtain the susceptibility at $T > \theta_F$:

$$x = \frac{M_A + M_B}{B_a} = \frac{(C_A + C_B)T - 2\mu C_A C_B}{T^2 - \theta_F{}^2} \qquad (2.7)$$

This is more complicated than the Curie – Weiss law for Ferro magnets at $T > \theta_F$. The plot of $\dfrac{1}{\chi}$ against T is shown in Fig- 2.4. It is to be noted that the reciprocal ferrimagnetic susceptibility shows considerable curvature as the temperature approaches θ_F and becomes infinite at θ_F.
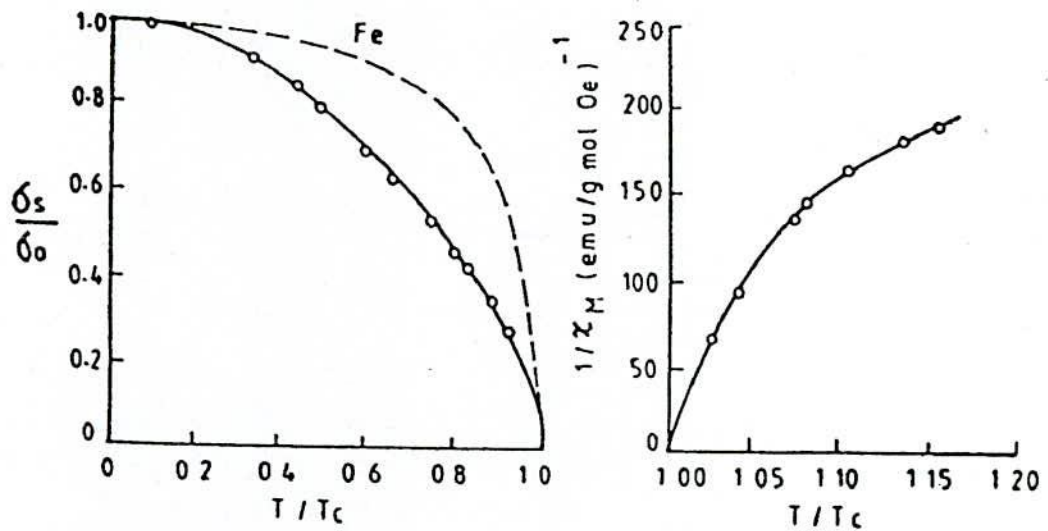
Figure-2.3: Thermal variation of the magnetic properties of a typical ferromagnetic. The fractional specific magnetization $\dfrac{\sigma_s}{\sigma_0}$ in ferromagnetic region is according to Pauthenet [7] and the reciprocal molecular susceptibility $\dfrac{1}{\chi_M}$ in the paramagnetic region is according to Serres [8](the dashed curve at left applies to metallic iron).
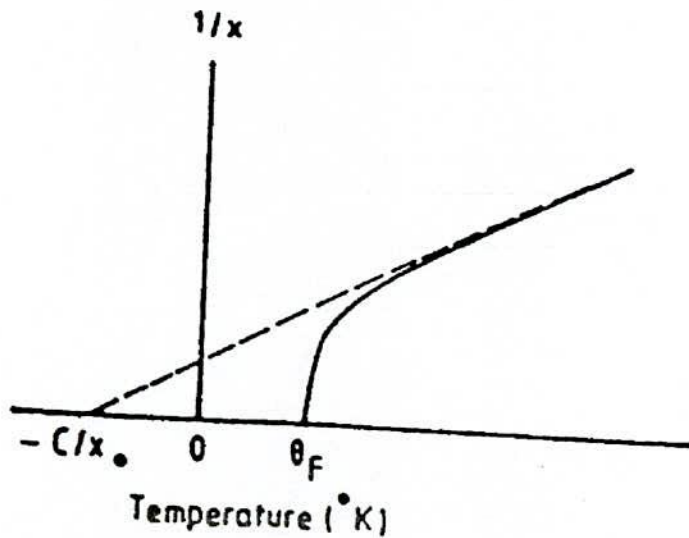
Figure-2.4: Theoretical variation of the reciprocal susceptibility with temperature for a ferrimagnetic above the Currie point.

15

2.3   Types of Ferrites

Ferrites are complex magnetic oxides that contain the ferric oxide (Fe_2O_3) and their basic magnetic component.

The general chemical composition can be written as $MO.Fe_2O_3$, where M represents a divalent metal ion such as Ni, Mn or Zn. The crystallographic of ferrites fall in a natural manner into three types: (i) the cubic ferrites of spinel type, (ii) The cubic ferrites of the garnet type and (iii) the hexagonal ferrites. The magnetic ferrites fall into two groups of different crystal structures as shown below:

```
                    ┌─────────────┐
                    │   FERRITE   │
                    └──────┬──────┘
            ┌──────────────┴──────────────┐
    ┌───────────────┐            ┌───────────────────┐
    │    CUBIC      │            │    HEXAGONAL      │
    │ e.g. MO. Fe2O3│            │ e.g. BaO.6Fe2O3   │
    └───────┬───────┘            └───────────────────┘
      ┌─────┴──────────────┐
┌──────────────┐   ┌──────────────────────┐
│   SPINEL     │   │      GARNET          │
│ e.g. MgAl2O4 │   │ e.g. 3MnO. Al2O3. 3SiO2│
└──────────────┘   └──────────────────────┘
```

FERRITE

CUBIC
e.g. $MO. Fe_2O_3$

HEXAGONAL
e.g. $BaO.6Fe_2O_3$

SPINEL
e.g. $MgAl_2O_4$

GARNET
e.g. $3MnO. Al_2O_3. 3SiO_2$
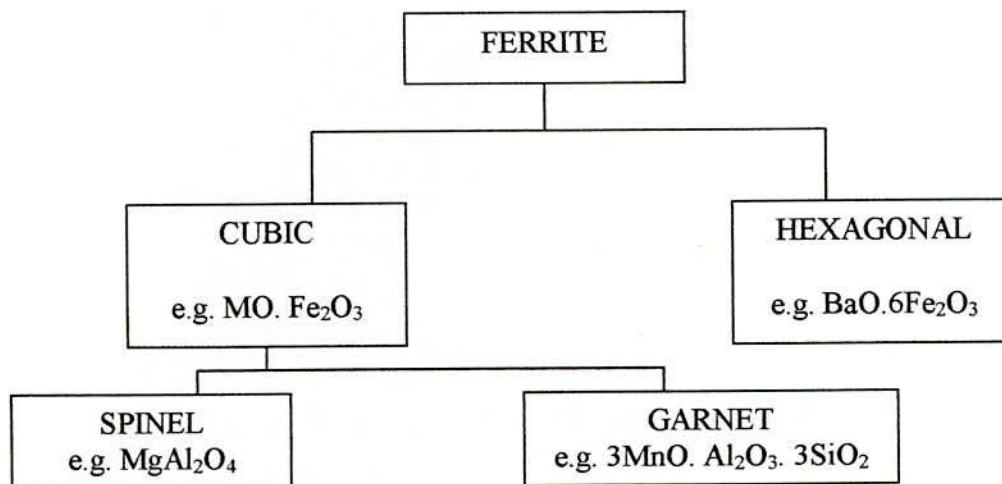
2.3.1   The cubic ferrites of the spinel type

These ferrites are also called ferrospinels because they crystallize in the same crystal structure as the mineral spinel and they derive their general formula MFe_2O_4 from the mineral spinel having composition $MgAl_2O_4$. In this formula, M represents a divalent ion of metal. Besides the divalency, another condition to qualify a metal in ferrospinels is its ionic radius which should fall between 0.6 and 1.0 A. Mg, Fe, Co, Ni, Cu, Zn and Cd all satisfy these two conditions and thus form various single cubic ferrites. Magnetite, which contains one ferrous ion and two ferric ions in each formula unit is a typical ferrite.

The crystal structure of ferrites is based on a face-centered cubic lattice of the oxygen ions. Each unit cell contains eight formula units. Therefore, there are $32O^{2-}$ anions, $16 Fe^{3+}$ cations and $8 M^{2+}$ cations in the cell, and the lattice constant is rather large, of the order of 8.5 Å. In each unit cell, there are 64 tetrahedral, or A-sites and 32 octahedral, or B-sites. These sites are so named because they are surrounded by four and six oxygen ions at equal distances, respectively.

2.3.2 The cubic ferrites of the garnet type

The mineral garnet refers to a group of mixed oxides, of which the widely known one has the chemical formula $Mn_3Al_2Si_3O_{12}$, or equivalently, $3MnO.Al_2O_3.3SiO_2$. Single magnetic garnets have the general formula $3M_2O_3.5Fe_2O_3 = 2M_3^{III} Fe_5^{III} O_{12}$. Note that, in magnetic garnets, the 24 positive charge units per formula units are divided unequally between the ferric ions (15 units) and another species of trivalent ions (9 units). Technically useful garnets are those with M = Sm, Eu, Gd, Tb, Dy, Ho, Er, Tm, Yb, or Y.

They are known as the rare-earth garnets. A code system has been adopted to name them: REG stands for the rare-earth garnets, GdIG for the gadolinium –iron garnet ($Gd_3Fe_5O_{12}$), YIG for the yttrium-iron garnet ($Y_3Fe_5O_{12}$), etc. Garnets crystallize in the cubic system with two-fifths of the ferric ions forming a body-centered cubic lattice. Like the ferrospinels, the garnets, too, pack a large number (160) of ions in eight formula units into a unit cell. The lattice constant is $\approx$ 12.5 Å, about 50% larger than those of ferrospinel. Also, the crystal structure of garnets is more complicated than the spinel structure because of the size (0.85 – 1.10 Å) of the M^{III} ions. They are too large to be accommodated at the interstitial sites between the oxygen ions. Hence the oxygen ions are prohibited from forming a close-packed structure as in the spinel. In each until cell, which contains eight formula units, there are three kinds of cation sites, of which

16 octahedral [a] sites are occupied by Fe^{III} ions,

24 tetrahedral (d) sites are also occupied by Fe^{III} ions and

24 dodecahedral {c} sites are occupied by M^{III} ions [9].

17

2.3.3 The hexagonal ferrites

The third type of ferrites is often called the barium ferrites because these compounds usually contain BaO, in additional to Fe_2O_3, as the basic component oxide. They are also known as the magnetoplumbites. The common chemical formula of barium ferrites is $l(BaO) \cdot m(MO) \cdot n(Fe_2O_3)$, or $Ba_l^{II} M_m^{II} Fe_{2n}^{III} O_{l+m+3n}$ where l, is much more complex than the previous two in both composition and crystallography. There are four ways in which the composition of barium ferrites may be changed. One is to vary the M^{II} ions. Mg, Mn, Fe, Co, Ni, Cu and Zn are found suitable for the formation of hexagonal ferrites. Another way is to alter the values for l, m and n. Basic combinations are found at 1–0–6 (the ferrite is designated M), 1–2–8(M_2W), 2–2–6(M_2Y) and 3–2–12(M_2Z). Compounds formed under these combinations are termed classical hexagonal ferrites. Still another way is to substitute for Ba with Pb or Sr and (or) substitute for Fe with Al, Ga, Cr or Mn. A fourth way to vary the composition of the barium ferrites is to mix two or more of the classical hexagonal ferrite in different proportions.
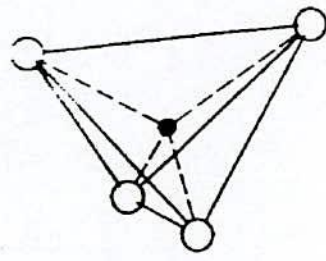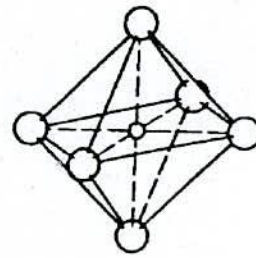
(a) Tetrahedral *A* site   (b) Octahedral *B* site

● Metal ion in tetrahedral site

○ Metal ion in octahedral site

◯ Oxygen ion

(c)

(d)
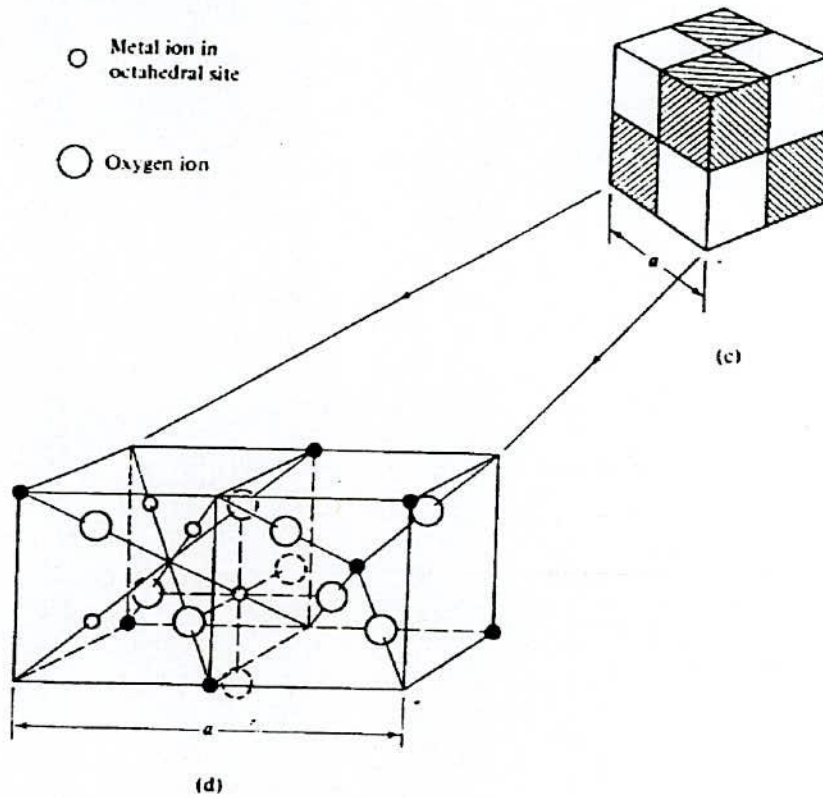
Figure -2.5 : Crystal structure of a cubic ferrite.

References:

[1] A. K. M. Abdul Hakim, Ph.D Thesis, Baangladesh University of Engineering and Technology, 1995.

[2] David Jiles, Introduction to Magnetism and Magnetic Materials, Chapman & Hall (1991)111.

[3] B. D. Cullity, Introduction to Magnetic Materials, Addison- Wesley Publishing Com. (1972)181.

[4] W. P. Wolf, Ferrimagnetism, Reports on Progress in Physics Vol. xx1v (1961)213.

[5] Y. Yafet and C. Kittel, Phys. Rev. **87** (1952).

[6] J. B. Goodenough, J. Phys. Chem. Solids, **6**(1958)287.

[7] Pauthenet, R., "Aimantation Spontanee de Ferrites," Annales de Physique, 7(1952) 710-745.

[8] Serres, A., "Recherches sur les Moments Ato miques," Annales de Physique,**17** (1932)5- 95.

[9] C.W. Chen, Magnetism and Metallurgy, of Soft Mag. Mat. , North - Holland Pub. Com. **XV**(1977)288.

CHAPTER -III

Specimen Preparation

3.1. Specimen Preparation

3.1.1. Methodology of Ferrite Preparation

The preparation of polycrystalline ferrites with optimum desired properties is still a complex and difficult task. Knowledge and control of the chemical composition, homogeneity and microstructure are very crucial. The preparation of polycrystalline ferrites with properties optimized has always demanded delicate handling and cautious approach. As the most of the properties needed for ferrite applications are not intrinsic but extrinsic, preparation of samples has to encounter added complexity. The ferrite is not completely defined by its chemistry and crystal structure but also requires knowledge and control of parameters of its microstructure such as density, grain size, porosity and their intra- and intergranular distribution. It is well known that almost all ferrites decompose at the elevated temperature if we want to melt them under normal conditions. This happens because the oxygen splits off at higher temperature reducing Fe^{3+} to Fe^{2+}. This necessarily implies that ferrite preparation by melting, as in case of metals, is not possible. The normal methods of preparation of ferrites comprise the conventional ceramic method or powder metallurgy, chemical co-precipitation method and sol-gel method. In this thesis work conventional ceramic method has been employed for the preparation of Ni-Cd ferrite for its relative simplicity and availability. The powder preparation process and sintering facility available at the Materials Science Division, Atomic Energy Centre, Dhaka, has been utilized for the preparation of samples. General formula of the sample is: $Ni_{1-x}Cd_xFe_2O_4$ where x = 0.0, 0.1, 0.2, 0.3, 0.4, 0.5, 0.6 and 0.8. The composition in weight percentages of different samples with varying x are shown in Table-1. The properties of Ni-Cd samples are influenced considerably by sintering temperature and compositions.

Table-1 : Composition of $Ni_{1-x}Cd_xFe_2O_4$ ferrites.

Cadmium content, x	weight% of NiO	weight% of CdO	weight% of Fe_2O_3
0.0	31.87	0	68.13
0.1	28.04	05.36	66.60
0.2	24.37	10.48	65.15
0.3	20.87	15.38	63.75
0.4	17.51	20.07	62.42
0.5	14.29	24.58	61.13
0.6	11.20	28.90	59.90
0.8	05.39	37.04	57.57

3.1.2. Method of Preparation

The general preparation procedure of ferrite comprises of the following operations as shown in the block diagram below and the detail of which are described subsequently.
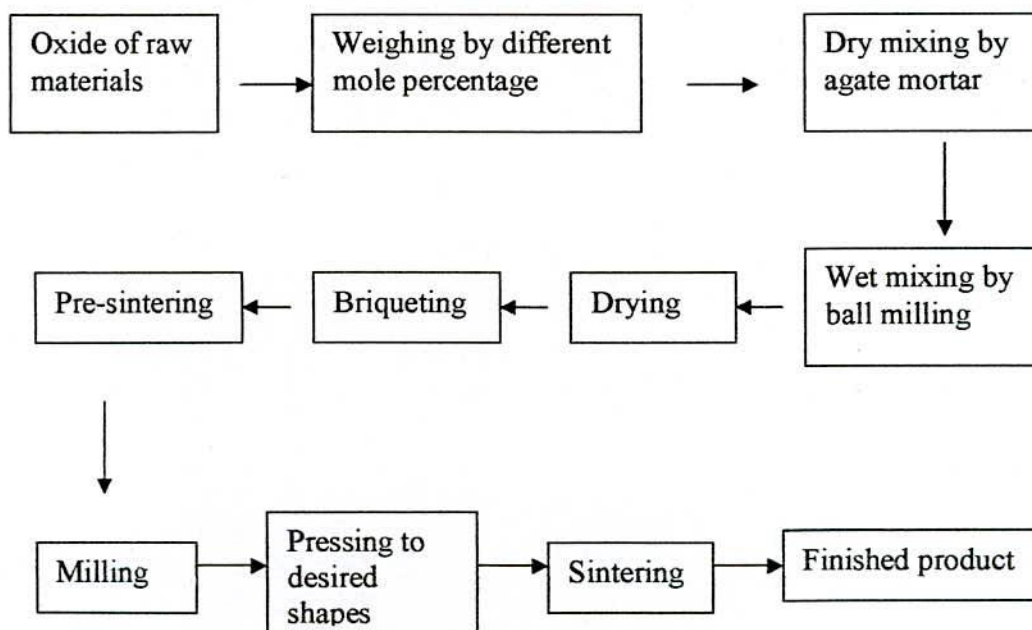
As a whole the preparation procedure generally consists of four major steps:

1. Preparing a mixture of materials with the cations in the ratio corresponding to that in the final product.
2. Prefiring the mixture to form ferrite.
3. Converting the 'raw' ferrite into powder and pressing the powder into the required shapes.
4. Sintering to produce a highly densified product.

One thing is to be remembered that, the sintering process is irreversible in terms of microstructure so that constant care must be maintained to keep conditions constant prior to and during sintering.

The following discussion will cover the important features of each step.

1. Preparing a mixture of materials having the right ratio of cations

The extend of the work in this step varies greatly, depending on the starting materials. When component oxides are used, the corresponding step involves a mere mixing of the oxides by wet milling. To avoid iron contamination, mixing is done with stainless steel balls in a steel ball milling machine and a fluid such as distilled water or acetone/ethanol is used to prepare the mixture into slurry.

The raw materials for the preparation of Ni-Cd ferrite were oxides of iron, nickel and cadmium. The purity of raw materials used in the present work are analytical research grade oxides as supplied by the manufacturer E. Mark of Germany. The constituent in required stoichiometric proportions were weighed first and then thoroughly mixed using ceramic mortar and pestle. The resultant powder was then ball milled for 6 hours to produce fine powders of mixed constituents.

2. Prefiring the mixture to form ferrite

The slurry prepared in step 1 is dried, palletized and then transferred to a porcelin crucible for prefiring at temperature between 1100°C and 1250°C. This was performed in a furnace named Gallen Camp at AECD. As far as the final composition of the ferrite is concerned step-2 is most crucial because subsequent steps would not change the composition substantially. For this reason, it is important to understand how a ferrite is formed from its component oxides. Few detail studies have reported on formation on Ni-Cd ferrite prepared by conventional ceramic methods [1-8].

The solid state reaction leading to the formation of ferrites actually achieved by counter diffusion. This means that the diffusion involves two or more species of ions which move in opposite direction initially across the interface of two contacting particles of different component oxides. In 1965 Carter and Kooy [9-10] made careful studies of the position of inter markers in diffusions couples and computed that the counter diffusion essentially involves the movement of cations through a more or less rigid lattice of oxygen anions.

During the prefiring stage, the reaction of Fe_2O_3 with metal oxide(say, MO or M'_2O_3) takes place in the solid state to form spinel according to the reactions:

$$MO + Fe_2O_3 \longrightarrow M Fe_2O_4 \text{ (spinel)}$$

$$2 M'_2O_3 + 4 Fe_2O_3 \longrightarrow 4 M' Fe_2O_4 \text{ (spinel)} + O_2$$

The NiO creep into Fe_2O_3 as below, to form an intermediate phase $Ni Fe_2O_4$ at low temperature:

$$Fe_2O_3 + NiO \longrightarrow Ni Fe_2O_4$$
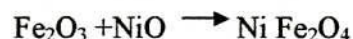
After that Cd ions are introduced by

$$(1-x)Ni Fe_2O_4 + x.CdO + x.Fe_2O_3 \longrightarrow Ni_{1-x}Cd_x Fe_2O_4$$
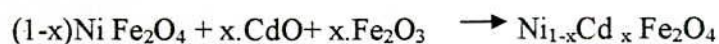
The mechanism just described for the formation of ferrites justifies the separate prefiring and sintering steps taken in the preparation procedures. The ferrite is formed essentially in step 2

but the raw ferrite thus formed has poor qualities. In order to produce chemically homogeneous and magnetically better material this prefired lump material was crushed. This oxide mixture was then milled thoroughly for 6-8 hours to obtain homogenous mixture. It is to be mentioned that the grain size can be reduced to ≈1micron by prolong normal ball milling. However some fraction of the particles in that case may be reduced to even sub micron level.

3. Converting the raw ferrite into powder and pressing the powder

Besides reducing the particle size to ≈1micron, grinding also eliminates intra particle pores and homogenizes the ferrite by mixing. To promote successful sintering in the next steps, the powder must be well characterized after grinding with respect to such factors as particles size and distribution, particle shape, homogeneity, absorbed gases, impurities and intraparticle porosity. Iron contamination due to continuous wear of the mill wall and steel ball need to be closely watched and minimized. Now to the ground homogeneous powder polyvinyl alcohol is added as a binder. Pressing the powder into compacts of desired shapes is done either by conventional method in a die-punch assembly or by hydrostatic or isostatic compaction.
We made use of the former one. Pressing a uniformly dense body by this method is difficult owing to the friction gradient of the powder at the walls of the die and between the particles themselves. This problems is somewhat overcome by the addition of external and internal lubricant to the powder such as stearic acid. Mainly, we made two types of samples- cylindrical and toroidal. Specimen was prepared by a hydraulic press with a pressure of 2 ton/cm^2 bar. The die was designed and made in the workshop of AECD. This is made of nonmagnetic stainless steel.

4. Sintering

This is a heat treatment by which a mass of compacted powder is transformed into a dense object. As the final major step in the preparation of ferrite products sintering must fulfill three requirements: (1) to bond the particles together so as to impart sufficient strength to the products; (2) to densify the green compacts by eliminating the pores and (3) to homogenize the materials by completing the reactions left unfinished in the preferring step [11]. The first two requirements are closely related as far as their mechanisms are concerned. For instance, as shown in Fig. 3.1 a simple way to bond two spherical particles is to form a neck at the contact by volume diffusion.

(a)   (b)
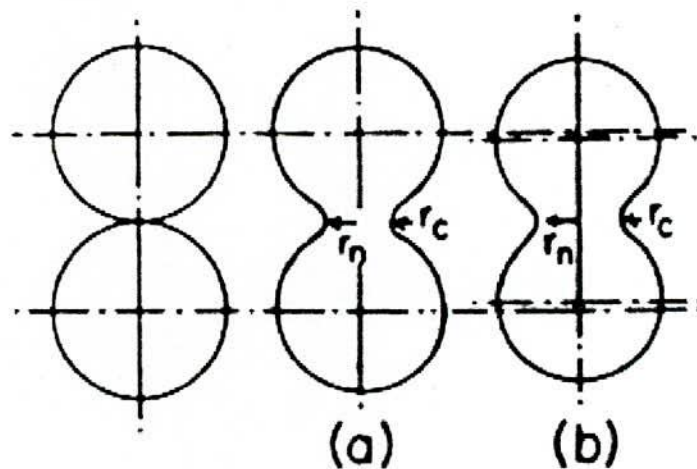
Figure-3.1 : Neck formation during sintering of spherical particles : (a) when there is no overall shrinkage and (b) when shrinkage occurs.

The formation of necks is also a key process leading to the shrinkage of pores. Precisely how pores disappear during sintering has long been a subject of intensive investigation. The theory has been changed from the traditional, but now obsolete, theory based on the reduction of surface energy as the driving force for eliminating the pores, through the

27

microcreep diffusion theory of Naborro and Herring to the current theory of Kuczynski [1961][12]. The current theory emphasizes the formation of necks as a key step in bonding the particles and in eliminating the pores and considers volume diffusion under surface tension as the main mechanism of neck formation. Other processes, such as plastic flow, surface or grain-boundary diffusion and evaporation-condensation, could play important supporting roles. On the basis of volume diffusion induced under surface tension, an important equation for the initial stage of the sintering process is given by

$$\frac{\Delta L}{L} = \left[\left(\frac{AD^* \gamma \Omega}{\bar{r}^3 kT} \right) t \right]^{-\frac{1}{2}}$$ (3.1)

where $\frac{\Delta L}{L}$ is the shrinkage of the compact, Ω the volume of a single vacancy, D^* the coefficient of self-diffusion for the slowest moving species, γ the surface energy, $\bar{r}$ the average radius of the particles, t the sintering time and A a constant, of the approximate value of unity. The above equation indicates that sintering fulfills requirements (1) and (2) more efficiently when the compact features high surface energy and self diffusivity and the particles are fine. For densification, Burke [1959] [13] made two important observations. One is that the formation of necks only marks the initial stage of sintering; an intermediate stage begings when grain growth occurs with the compact density at around 60% of the theoretical value and ends when the pore phase becomes discontinuous and the density reaches a value of $\approx$ 95%. Another observation of Burke deals with the final stage of sintering. If discontinuous grain growth occurs after the intermediate stage, migration of grain boundaries will leave the remaining isolated pores trapped inside the grains, thus preventing further shrinkage of these intra particle pores and practically stopping the sintering process. In this operation, the cooling rate plays an important role on which the structural modification is mainly based. Sintering of crystalline solids follows the following empirical relationship regarding rate of grain growth [14]:

$$\bar{d} = kt^n$$ (3.2)

28

where $\bar{d}$ is the mean grain diameter, t is sintering time, n is about $\frac{1}{3}$ and k is a temperature dependent parameter.

For sintering our samples, we used a programmable furnace NABER (Model-HT 08/16 Germany) at AECD. The temperature of the furnace could be maintained within an accuracy of $\pm 1^0C$.

For sintering we followed more or less the following programme :

| Weight measurement | $\longrightarrow$ | Wet milling for 2 hours | $\longrightarrow$ | dried and shaped into disc & ring |

Dried sample pre-sintered at 900^0C for a holding & time of 5 hours 40 minutes.

| Centrifugal ball milling | $\longleftarrow$ | Hammering | $\longleftarrow$ | Dried sample pre-sintered at 900^0C for a holding & time of 5 hours 40 minutes. |

| Dried and shaped into disc & ring | $\longrightarrow$ | Sintering at temperature of 1100^0C to 1250^0 at an interval of 50^0C for 8 hours and holding time is 4 hours for each sample. |

References :

[1] U. Konig, Tech. Mitt. Krupp-Forsch. Ber. **32**(1974)75.

[2] E. Roess, Ferrites, Proc. Intern. Conf. Japan (1980)203.

[3] G. C. Kuezynski, Ferrites, Proc. Intern. Conf. Japan (1970)87.

[4] P. Reijnin, Science of Ceramics, Ed. G.H.Stewart, Academic Press, London, **3**(1967).

[5] J. F. Dunean, K. J. D. Mckenzie and D. J. Stewart, The Mossbauer Effect, Symp. Faraday Soc. **1**(1967)103.

[6] M. Zaharescu, M. Balasoin, M. Crisan, T. Tavala and V. Moser, Rev. Roum. Chim. **29**(1984)247.

[7] P. Nauber and C. Michalk, Hermsderfer Techn. Mitt. **25**(1985)2152.

[8] A. Chiba and O. Kimura, J. Japan. Soc Powder and Powder Mat. **31**(1984)75.

[9] R. E. Carter, J. An. Ceramic Soc. **44**(1961)116.

[10] C. Kooy, 5th Int. Symp. React. In Solids (Elsevier, Amsterdam)(1965)21.

[11] C.W. Chen, Magnetism and Metallurgy, of Soft Mag. Mat. , North - Holland Pub. Com. **XV**(1977)288.

[12] Kuezynski, G. C. , Powder Metallurgy, Lesynski, w. ed. (Interscience, NY) **11**(1961).

[13] Burke, J. E., Kinetics of High-Temperature Processes, Kingery, W.D.,ed.(Wiley,NY)1959.

[14] P. I. Slick, Ferrites for Non-microwave Applications, ferromagnetic materials, Ed.E.P.Wolfarth, North Holland Pub. Co. **2**(1980).

CHAPTER - IV

Experimental Measurements

4.1 The X-ray Diffraction

The x-ray diffraction (XRD) provides precise knowledge of the lattice parameter as well as the substantial information on the crystal structure of the material under study. XRD is one of the most effective tools for the determination of the atomic arrangement in a crystal.

X-rays are the electromagnetic waves whose wavelengths are in the neighborhood of 1O. The wavelength of an X-ray is thus of the same order of magnitude as the lattice constant of crystals, and it is this which makes X-rays so useful in structural analysis of crystals.

Whenever X-rays are incident on a crystal surface, they are reflected from it. This is Bragg reflection. Bragg reflection is a coherent elastic scattering in which the energy of the ray is not changed on reflection. If a beam of monochromatic radiation of wavelength λ incidents on a periodic crystal plane at an angle θ and is diffracted in the same angle, this event abides by the celebrated Bragg's law which is given below

$$2d\sin\theta = n\lambda \tag{4.1}$$

Here d is the distance between crystal planes, and n is positive integer. Bragg's law also suggests that the diffraction is only possible when $\lambda < 2d$ [1].

X-ray diffraction (XRD) is a versatile non-destructive analytical technique for identification and quantitative determination of various crystalline phases of powder or solid samples of any compound. A PHILIPS X Pert PRO X-ray diffraction system was used to get X-ray data for the samples at the Materials Science Division, Atomic Energy Center, Dhaka, which is a sophisticated X-ray diffractometer installed very recently and shown in Fig. 4.1. The powder diffraction technique was used with a primary beam power of 40 kV and 30mA for Cu radiation. A nickel filter was used to reduce Cu-K$_\alpha$ radiation and finally Cu-K$_\alpha$ radiation was only used as the primary beam. A (θ - 2θ) scan was taken from 15° to 75° to get possible fundamental peaks of the sample with the sampling pitch of 0.02° and time for each step data

32

collection was 1.0 sec. Both the programmable divergence and receiving slits were used to control the irradiated beam area and output intensity from the sample respectively.
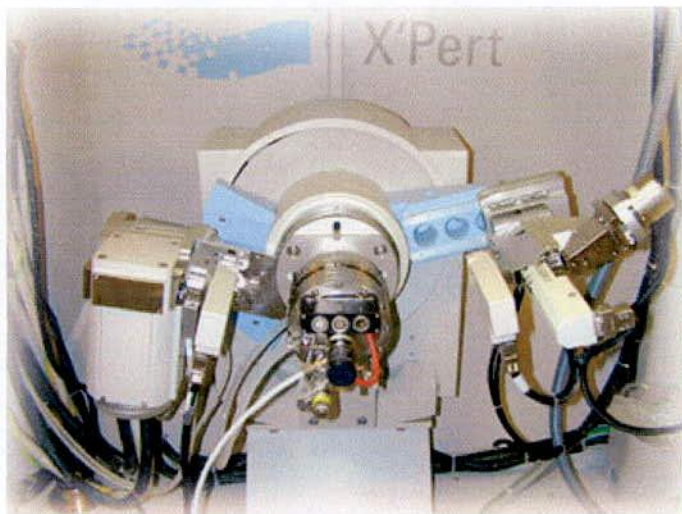
Fig. 4.1: Internal arrangement of a PHILIPS X Pert PRO X-ray diffractometer.

An anti-scatter slits were used just after the sample holder to reduce air scattering. Two solar stills were used just after the tube and in front of the detector to get parallel beam only. All the data of the samples were stored in the computer memory and later analyzed using computer software "X PERT HIGHSCORE". For each composition, the cylindrical samples of weight more than 2 gm are converted into powder. For XRD experiment each sample was set on a glass slide and fixed the sample by putting adhesive tape at the two ends of the sample.

4.1.1   Interpretation of the XRD Data :

The XRD data consisting of θ_{hkl} and d_{hkl} values corresponding to the different crystallographic planes are used to determine the structural information of the samples like lattice parameter and constituent phase.

Lattice parameters of Ni-Cd ferrites samples were determined. Normally, lattice parameter of an alloy composition is determined by the Debye-Scherrer method after extrapolation of the curve. In this method, at least five fundamental reflections are required to determine lattice parameter. In the present case, ten reflection planes are prominent in all XRD patterns and we would like to understand how the value of lattice parameter changes with the increase of Cd content in the Ni-Cd ferrites. We determine the lattice spacing (inter planer distance), d using these reflections from the equation:

$$2d \sin \theta = \lambda \quad \text{i.e.} \quad d = \frac{\lambda}{2 \sin \theta} \tag{4.2}$$

The lattice parameter for each peak of each sample was calculated by using the formula:

$$a = d_{hkl} \times \sqrt{h^2 + k^2 + l^2} \tag{4.3}$$

Where h, k and l are the indices of the crystal planes. We get d_{hkl} values from the computer using software "X PERT HIGHSCORE". So we got ten 'a' values for ten reflection planes such as a_1, a_2, a_3 etc.

To determine the exact lattice parameter for each sample, Nelson-Riley method was used. The Nelson-Riley function $F(\theta)$, can be written as

$$F(\theta) = \frac{1}{2} \left(\frac{\cos^2 \theta}{\sin \theta} + \frac{\cos^2 \theta}{\theta} \right) \tag{4.4}$$

Now drawing the graph of 'a' vs $F(\theta)$ and using linear fitting of those points will give us the lattice parameter a_0. This is the value of 'a' at $F(\theta)=0$. These a_0's are calculated within an error estimated to be ± 0.0001 Å.

4.1.2 X- Ray density and bulk density determination:

X-ray density ρ_x was also calculated using the lattice parameter. The relation between ρ_x and a is as follows:

$$\rho_x = \frac{8M}{Na^3} \, g/cm^3 \tag{4.5}$$

Where N is the Avogadro's number (6.02×10^{23} mol^{-1}), M is the molecular weight.

The bulk density , ρ_B is measured by the formula:

$$\rho_B = \frac{M}{V} \qquad (4.6)$$

4.1.3 Porosity determination:

The difference between the bulk density, ρ_B (measured by usual mass and dimensional consideration) and theoretical density, ρ_x gave us the measure of porosity. Porosity (P) in percentage will be calculated using the following equation [2] :

$$P = \left(1 - \frac{\rho_B}{\rho_x}\right) \times 100\% \qquad (4.7)$$

4.2 Curie temperature (T_c) measurement

Curie temperature measurement is one of the most important measurements regarding magnetism. Curie temperature provides substantial information on magnetic states of a substance in respect of the strength of exchange interaction. So, the determination of accurateCurie temperature accurately is of great importance.

Curie temperature measurements were done by using WAYNE KERR IDUCTANCE ANALYZER 3255B, a small oven and a thermocouple based thermometer. We made use of the excellent experimental facilities available at Materials Science Division, AECD. The temperature dependent permeability was measured by using induction method. The specimen formed the core of the coil. We used a 100 kHz AC signal of 100 mV. By varying temperature, inductance of the coil as a function of temperature was measured. Dividing this value by L_0 (inductance of the coil without core material), we got the permeability of the core i.e. the sample. When the magnetic state inside the ferrite sample changes from ferromagnetic to paramagnetic, the permeability falls sharply. From this sharp fall at specific

35

temperature the Curie temperature is determined. This is the basic principle used in our experimental set up.

The number of turns in each coil is 5. The sample thus wound is kept in the middle position of a tubular oven with a thermocouple placed close to the sample. The thermocouple measures the temperature inside oven and also of the sample. The sample is kept just in the middle part of the cylindrical oven so that gradient is minimized. The temperature of the oven is raised slowly. If the heating rate is very fast then temperature of the sample may not follow the temperature inside the oven and there can be misleading information on the temperature of the samples. The thermocouple showing the temperature in that case will be erroneous. Due to the closed winding of wires the sample may not receive the heat at once. So, a slow heating rate can eliminate this problem. Also a slow heating ensures accuracy in the determination of Curie temperature. The oven was kept thermally insulated from the surroundings. Actually Curie Temperature was measured from the temperature dependence of initial permeability.

4.3 Permeability Measurement

For high frequency application, the desirable property of a ferrite is the high permeability with low loss. The present goal of most of the recent ferrite researchers is to fulfill this requirement. Before going into the complexity of permeability measurement, we take a detour through the theories and mechanisms involved in permeability.

4.3.1 Theories of Permeability:

Permeability is namely defined as the proportional constant between the magnetic field induction B and applied intensity H:

$$B = \mu H \tag{4.8}$$

This naïve definition needs further sophistications. If a magnetic material is subjected to an AC magnetic field as given below:

$$H = H_0 e^{i\omega t} \tag{4.9}$$

then it is observed that the magnetic flux density B experiences a delay. The delay is caused due to presence of various losses and is thus expressed as

$$B = B_0 e^{i(\omega t - \delta)} \qquad (4.10)$$

where δ is the phase angle and marks the delay of B with respect to H. The permeability is then given by

$$\mu = \frac{B}{H} = \frac{B_0 e^{i(\omega t - \delta)}}{H_0 e^{i\omega t}}$$

$$= \frac{B_0 e^{-i\delta}}{H_0} = \mu' - i\mu'' \qquad (4.11)$$

$$\text{Where, } \mu' = \frac{B_0}{H_0}\cos\delta, \ \mu'' = \frac{B_0}{H_0}\sin\delta \qquad (4.12)$$

The real part μ' of complex permeability μ as expressed in equation (4.12) represents the component of B which is in phase with H, so it corresponds to the normal permeability. If there are no losses, we should have $\mu = \mu'$. The imaginary part μ'' corresponds to that part of B which is delayed by phase angle ranging upto 90^0 from H. The presence of such a component requires a supply of energy to maintain the alternating magnetization, regardless of the origin of delay.

The ratio of μ'' to μ', as is evident from equation (4.12) gives

$$\frac{\mu''}{\mu'} = \frac{(B_0/H_0)\sin\delta}{(B_0/H_0)\cos\delta} = \tan\delta \qquad (4.13)$$

This tanδ is called the Loss Factor or Loss tangent. The Q-factor or quality factor is defined as the reciprocal of this loss factor, i.e.

$$Q = \frac{1}{\tan\delta} \qquad (4.14)$$

4.3.2 Mechanisms of permeability:

The mechanisms can be explained as follows: a demagnetized magnetic material is divided into number of Weiss domains separated by block walls. In each domain all the magnetic moments are oriented in parallel and the magnetization has its saturation value M_s. In the

37

walls the magnetization direction changes gradually from the direction of magnetization in one domain to that in the next. The equilibrium positions of the walls result from the interactions with the magnetization in neighboring domains and from the influence of pores, crystal boundaries and chemical inhomogeneities which tend to favor certain wall positions.

4.3.2.1 Wall permeability:

The mechanism of wall permeability arises from the displacement of the domain walls in small fields. Let us consider a piece of material in the demagnetized state, divided into Weiss domains with equal thickness L by means of 180^0 Block walls.(shown in fig. 4.2) The walls are parallel to the Y, Z plane. The magnetization M_s in the domains is oriented alternately in the +Z or –Z direction. When a field H with a component in the +Z direction is applied, the magnetization in this direction will be favoured. A displacement dx of the walls in the direction shown by the dotted lines will decrease the energy density by an amount:

$$\frac{2M_s H_z dx}{L}$$

This can be described as a pressure $2M_S H_Z$ exerted on each wall. The pressure will be counter acted by restoring forces, which for small deviations may be assumed to be $k.dx$ per unit wall surface. The new equilibrium position is then given by

$$d = \frac{M_s H_z dx}{L} \tag{4.15}$$

From the change in the magnetization

$$\Delta M = \frac{2M_s d}{L} \tag{4.16}$$

the wall susceptibility χ_ω may be calculated. Let H makes the angle θ with z direction. The magnetization in the θ direction becomes

$$(\Delta M)_\theta = \frac{2M_s d}{L} \theta \tag{4.17}$$

and with $H_Z = H \cos\theta$ and $d = \frac{2M_s H_z}{k}$ we obtain

38

$$\chi_\omega = \frac{(\Delta M)_\theta}{H} = \frac{4M_s^2 \cos^2 \theta}{KL} \qquad (4.18)$$
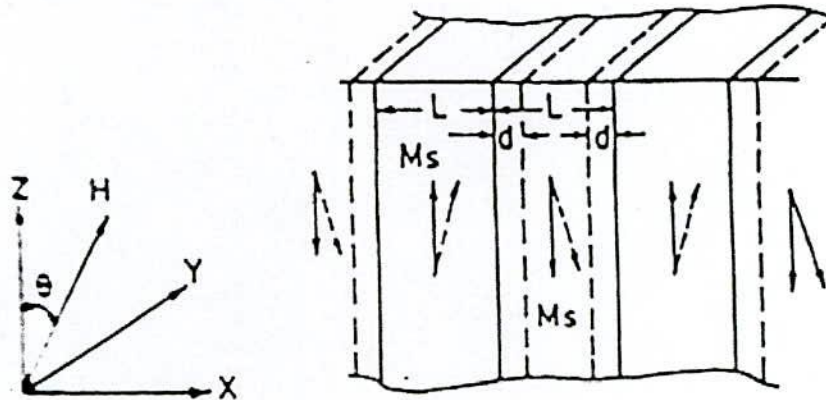
Figure 4.2: Magnetization by wall motion and spin rotation.

4.3.2.2. Rotational permeability :

The rotational permeability mechanism arises from rotation of the magnetization in each domain. The direction of M can be found by minimizing the magnetic energy E as a function of the orientation. Major contributions may be due to the stress and shape anisotropy. The stress may influence the magnetic energy via the magnetostriction. The shape anisotropy is caused by the boundaries of the sample as well as by pores, nonmagnetic inclusions and inhomogeneities. For small angular deviations α_x and α_Y or M, where

$$\alpha_x = \frac{M_X}{M_S} \ \& \ \alpha_Y = \frac{M_Y}{M_S}$$

From the equilibrium Z-direction may be expressed as

$$E = E_0 + \frac{1}{2\alpha_X^2 E_{XY}} + \frac{1}{2\alpha_Y^2 E_{YY}} \tag{4.19}$$

where it is assumed that X and Y are the principal axes of the energy minimum. Instead of E_{XX} & E_{YY}, the anisotropy field H_X^A and H_Y^A are often introduced. Their magnitude is given

by
$$H_X^A = \frac{E_{XX}}{2M_s} \text{ and } H_Y^A = \frac{E_{YY}}{2M_s} \tag{4.20}$$

H_X^A & H_Y^A represents the stiffness with which the magnetization is bound to the equilibrium direction for deviations in the X and Y direction, respectively. The rotational susceptibilities $\chi_{r,x}$ and $\chi_{r,y}$, for fields applied along X and Y directions, are $\chi_{r,x} = \frac{M_s}{H_X^A}$ and $\chi_{r,y} = \frac{M_s}{H_Y^A}$ respectively.

For cubic materials it is often found that H_X^A & H_Y^A are equal. For $H_X^A = H_Y^A = H^A$ and a field of H which makes and θ with Z-direction (as shown in fig. 4.2) the rotational susceptibility, $\chi_{r,c}$ in one crystallite becomes

$$\chi_{r,c} = \frac{M_s}{H^A \sin^2 \theta} \tag{4.21}$$

A polycrystalline material consisting of a large number of randomly oriented grains of different shapes, with each grain divided into domains in a certain way the rotational susceptibility χ_x of the material has to be obtained as a weighted average of $\chi_{r,c}$ of each crystallite, where the mutual influence of neighboring crystallites has to be taken into account. If the crystal anisotropy dominates other anisotropies, the H^A will be constant throughout the material. So only the factor $\sin^2 \theta$ (equation 4.21) has to be averaged. Snoek assuming a linear averaging of $\chi_{r,c}$, found the following relation:

$$\chi_r = \frac{2M_s}{3H^A} \tag{4.22}$$

The total internal susceptibility

$$\chi = \chi_\omega + \chi_r = \frac{4M_s^2 \cos^2 \theta}{KL} + \frac{2M_s}{3H^4} \qquad (4.23)$$

If the shape and stress anisotropies can not be neglected, H^4 will be larger. Any estimation of χ_r will rather uncertain as long as the domain structure and the pore distribution in the material are not known. A similar estimate of χ_ω would require knowledge of the stiffness parameter k and the domain width L. These parameters are influenced by the factors like, imperfection, porosity, crystallite shape and distribution of pores.

4.3.3 Techniques of measurements of permeability

Measurements of permeability normally involve the measurements of the change in self inductance of a coil in presence of the magnetic core. The behaviour of a self inductance can now be described as follows. Suppose we have an ideal lossless air coil of inductance L_0. On insertion of magnetic core with permeability μ, the inductance will be μL_0. The complex impedance Z of this coil can be expressed as

$$Z = R + jX = j\omega L_0 \mu = j\omega L_0(\mu' - j\mu'') \qquad (4.24)$$

where the resistive part is

$$R = \omega L_0 \mu' \qquad (4.25)$$

and the reactive part is

$$X = w L_0 \mu' \qquad (4.26)$$

The radio frequency (RF) permeability can be derived from the complex impedance of a coil Z (equation 4.24). The core is usually toroidal to avoid demagnetizating effects. The quantity L_0 is derived geometrically.

41

4.3.4 Measurement of frequency characteristics of Ni-Cd ferrite samples:

The frequency characteristics of the Ni-Cd ferrite samples i.e. the permeability spectra were investigated using a Hewlett Packard Impedance Analyzer of model no-4192A. The measurements of inductances were taken in the frequency range of 1 KHz to 13MHz. The values of measured parameters such as inductance and loss tangent were obtained as a function of frequency and the real and on the basis of the values imaginary part of permeability are calculated. μ' is calculated by using the following formula:

$$L_s = L_0 \mu' \tag{4.27}$$

and
$$\tan\delta = \mu''/\mu' \tag{4.28}$$

Where L_s is the self-inductance of the sample core and

$$L_0 = \frac{\mu_0 N^2 s}{\overline{d}} \tag{4.29}$$

where L_0 is the inductance of the winding coil without the sample core and N is the number of turns of coil (here N=5), s is the area of cross section of the toroid as given below

$$s = dh, \text{ where, } d = (d_1 \sim d_2)/2, \quad h = \text{height}$$

and $\overline{d}$ is the mean diameter of the sample given as follows:

$$\overline{d} = \frac{d_1 + d_2}{2} \tag{4.30}$$

4.4 Magnetization measurement

Magnetization is defined as the magnetic moment per unit volume. There are various ways of measuring magnetization of a substance. In the present thesis magnetization has been measured by using a vibration sample magnetometer (VSM) at room temperature, applying a wide range of magnetic field from - 600000 $A.m^{-1}$ to + 600000 $A.m^{-1}$.

These measurements were carried out at Atomic Energy Research Institute, Savar. We use Hirst VSM02 which is an automatic vibrating sample magnetometer for characterization of soft and hard magnetic materials manufactured by HIRST Magnetic

Instruments Ltd. A block diagram of a typical VSM system is shown in Fig.4.3. The Hirst VSM system arrangement is shown in the Fig. 4.4. The vibration and measuring unit of Hirst VSM is shown in Fig.4.5.

Description and brief working principle of VSM:

Vibrating Sample Magnetometers, as the name implies, vibrate the sample as part of the measurement process. This provides the Fluxmeter element of the system with the dynamic component which it requires to make the measurement. The applied field is changed so, at each measurement point the field is static and hence no eddy currents to cause problems.

The objective when using a VSM or any other type of magnetic characterization system is to obtain the dependence of the magnetization (J) on the applied field (H) -> J(H). Once this is obtained, many useful parameters can be extracted from the data. VSM typically generate the applied field (H) using an electromagnet or a super conducting solenoid for fields greater than 2.5-3 Tesla. The magnet is driven around its hysteresis curve by changing the applied field (H) and the J signal is determined.
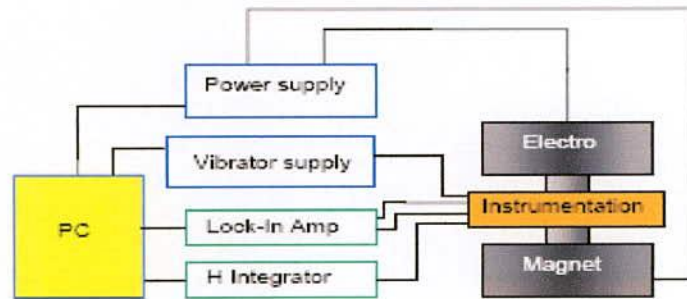
Fig.4.3: Block diagram of a VSM system.

Fig.: 4.4 Hirst VSM system arrangements.

Fig.4.5 Vibration and measurement unit

In the VSM02 a conventional electromagnet is implemented with two independent coils driven by independent 1000W amplifiers. The current control on the coils utilizes transconductance to ensure that constant current is supplied for a particular demand and to ensure that resistive changes due to heading do not cause the measurement to drift. The applied field (H) is measured using a hall element connected to a Gauss meter (BGM01).

The magnetization field (J) is determined by utilizing pickup coils. As with large iron poles and high inductances it is impossible to change the field quickly without causing unwanted effects. VSM measurements are a quasi-static process where the samples J field is determined when the applied field is static. As the applied field is static when J is determined, the J magnetization field is also static. Pickup coils work by faradays law of induction.

Where e is the voltage induced, d-theta is the change in magnetic flux in time t. As the J field is static there is no d-theta so a pickup coil cannot work. To overcome this problem the sample is vibrated using a sinusoidal oscillation. This vibration generates the required change in flux with respect to time and produces a signal from the pickup coils.

As the sample is vibrating at a known frequency with known phase it is possible to use a lock-in amplifier to extract the J value from the pickup coils output. This also has huge advantages as lock-in amplifiers can discriminate against noise and pick out a tiny signal buried in noise. This gives VSM's the potential to have huge gain on the J measurement channel. In the VSM02 the maximum J gain is approximately x 1,300,000. This allows very small samples, or samples with a small magnetic moment to be measured such as thin-films, powders and inks.

4.4 Resistivity Measurement

Resistivity of the samples has been measured using conventional two probe method, using pellet samples of 13-14 mm diameter and 2-3 mm thickness. Samples were prepared by sintering the samples at 1100°C , 1150°C and 1200°C for 4 hours. The samples were polished using metallurgical polishing machine with the help of silicon carbide polishing papers with grit size 600, 800 and 1200 successively. After that the samples were clean with acetone and then again polished with special velvet type polishing cloth named as alphagam for finer polishing using fine alumina powder of grain size 0.05 micron dispersed in a liquid. The powders are of various sizes starting with 1 micron down to 0.05 micron. Samples are then cleaned in a ultrasonic cleaner and dried in furnace at 150°C for several hours. Then the samples are again cleaned with acetone and silver paste was added to both the sides of the polished pellet samples together with two thin copper wires of 100 micron diameter for conduction. Again the samples are dried at 150°C to eliminate any absorbed moisture. Dc resistivity was measured using a Electrometer Keithley model 6514 at room temperature. The resistivity has been calculated using the formula :

$$R = \rho \frac{L}{A} \tag{4.31}$$

Where the symbols have their conventional meaning.

References:

[1] C.KIttel, Introduction to Solid State Physics, 7th edition, John Wiley & Sons,Inc.,Singapore (1996).

[2] B. D. Cullity, Introduction to Magnetic Materials, Addision-Wisley Publishing Company, Inc., California (1972).

Results and Discussion

5.1 X-Ray Diffraction (XRD)

Structural characterization and identification of phases is a prior for the study of ferrite properties. Optimum magnetic and transport properties of the ferrites necessitate to have single phase cubic structure. X-ray, neutron and electron diffraction are useful techniques to evaluate the various phases of the synthesized ferrites as well as their unit cell parameters. In the present study X-ray diffraction technique has been utilized to discern these parameters. Fig.5.1 shows the XRD pattern of all the samples of $Ni_{1-x}Cd_xFe_2O_4$.

The fundamental reflections from the planes of (220), (331), (222), (400), (422), (511), (440), (620), (533),and (622) characterizing the cubic spinel structures are observed. This indicates that the synthesized ferrite compositions are of single-phase cubic spinel since no ambiguous reflections other than the spinel structures are evidenced. This also demonstrates the homogeneity of the prepared samples. Fig. 5.2 shows the extended form of XRD pattern with cadmium content x=0.8. For the precise determination of lattice parameter, a_0, higher angle reflections as well as wavelength corresponding to $Cu-K\alpha_1$ and $Cu-K\alpha_2$ should be taken into consideration since they have different wavelengths and also they are manifested only in higher 2θ values. Fig.5.3 demonstrates the expanded form of Fig.5.2 of 2θ range from 51° to 56° in which $Cu-K\alpha_1(\lambda=1.540598$ Å) and $Cu-K\alpha_2$ ($\lambda=1.544426$ Å) are clearly displayed. The lattice parameter of all the samples have been precisely determined considering all the reflections together with the $Cu-K\alpha_1$ and $Cu-K\alpha_2$ components using the extrapolated Nelson Relay function $F(\theta) = 0$ [1]. The representative curves for Cd content x = 0.0, 0.3 and 0.6 of N-R function extrapolation are shown in Fig. 5.4. The least square linear fitting gives the precise lattice parameter as an intercept on the Y-axis. The lattice parameter thus determined

against Cd content is presented in Fig.5.5. and also shown in Table-5.2. From the Fig.5.5 it is observed that the lattice parameter increases linearly with increasing Cd content obeying Vegard's law [2].

The variation of lattice parameter a, against the concentration x, can be explained in terms of the larger ionic radius of Cd^{2+} ions (= 0.97Å) [3] which when substituted in the lattice resides on tetrahedral A-sites and displaces smaller Fe^{3+} ions (= 0.64Å)[3], from A-sites to octahedral B-sites. This also suggests that the Cd^{2+} ions have preference to occupy A-sites, similar with the case of Zn^{2+} ions, which show a preference for the tetrahedral A-sites of the spinel lattice [4]. It is well known that the distribution of cations in the octahedral B-sites and tetrahedral A-sites determines to a great extent the physical, electrical and magnetic properties of ferrites. There exist a correlation between the ionic radius and the lattice constant, the increase of the lattice constant is proportional to the increase of the ionic radius [5]. Thus the introduction of larger ions in the ferrite lattice results in an increase of the distance between the magnetic ions which facilitates the possibility of studying fundamental properties like Curie temperature and magnetization [6] as affected by distance dependence exchange interaction.

The least square linear fitting of lattice parameter, a_0 as a function of Cd content, x gives an empirical relation of the entire composition range of $Ni_{1-x}Cd_xFe_2O_4$ ferrites:

$$a_x = a_0 + 0.3665x \tag{5.1}$$

where, a_x is the lattice constant of a ferrite containing x mole of Cd, a_0 = 8.3344 Å is the lattice parameter of $NiFe_2O_4$ ferrite. From this empirical relation a_x (x = 1.0) i.e. for the $CdFe_2O_4$ has been calculated to be 8.7009 Å. Experimentally determined lattice parameter a

value in the present study for $NiFe_2O_4$ is 8.3344 Å has good coincidence with that of literature value 8.34 Å [7], 8.337 Å [8, 9] for $NiFe_2O_4$ and 8.70 Å [10, 11] , 8.68 Å [12] for $CdFe_2O_4$ ferrite against 8.7009 Å as found by calculation from the linear fitting equation.

Table-2 : Lattice parameter, molecular mass, theoretical density, bulk density and porosity for the samples with the composition $Ni_{1-x}Cd_xFe_2O_4$ sintered at 1200°C for 4 hours.

Cadmium content, x	Lattice parameter, a (Å)	Molecular mass, M	Theoretical density g/c.c.	Bulk density g/c.c.	Porosity
0.0	8.329	234.39	5.39	4.45	17%
0.1	8.371	239.762	5.43	4.59	15%
0.2	8.407	245.134	5.48	4.99	9%
0.3	8.451	250.506	5.51	5.08	8%
0.4	8.486	255.878	5.56	5.15	7%
0.5	8.521	261.25	5.61	5.29	6%
0.6	8.554	266.622	5.66	5.36	5%
0.8	8.622	277.366	5.75	5.38	6%

Density of the ferrite samples plays a vital role in the determination of magnetic as well as electrical properties. It is well known that high permeability could be achieved by increasing the density of the ferrites [7]. The theoretical density calculated from the determined lattice parameter and the bulk density measured from the ratio of mass and volume for the entire series of $Ni_{1-x}Cd_xFe_2O_4$ compositions are shown in Fig.5.6.
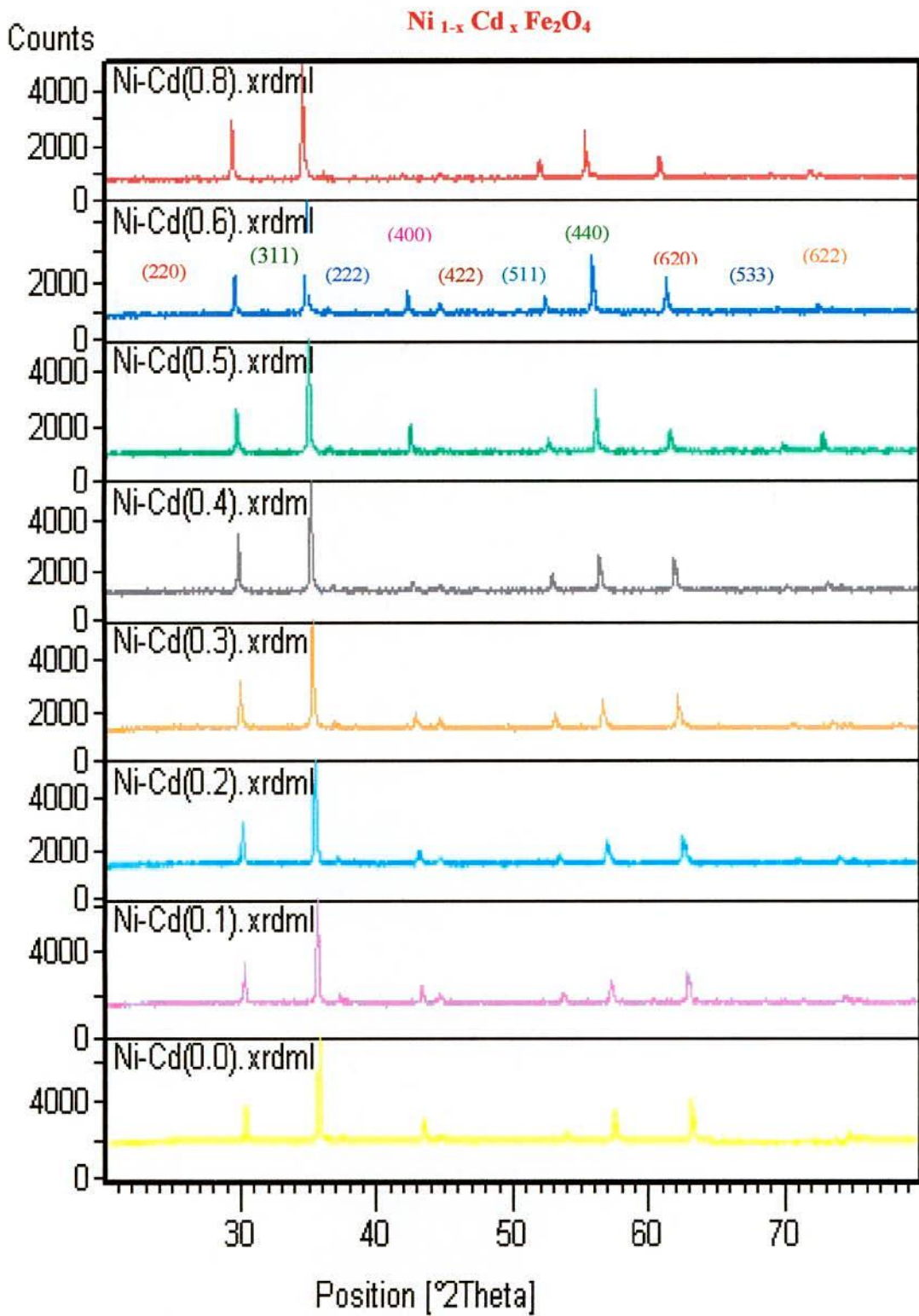
Fig. 5.1 X-Ray Diffraction (XRD) pattern of $Ni_{1-x}Cd_xFe_2O_4$ ferrite samples.
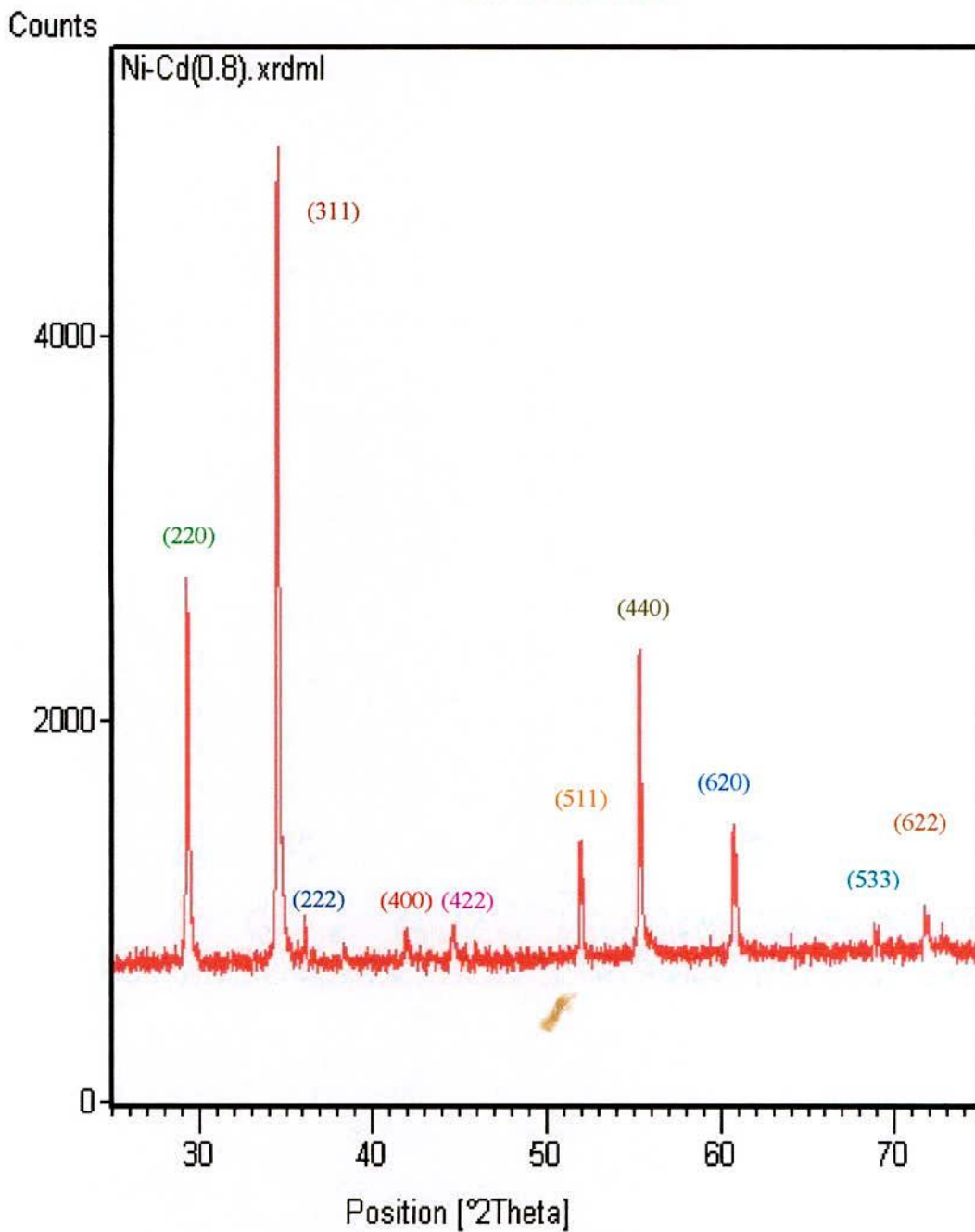
Ni $_{0.2}$ Cd$_{0.8}$ Fe$_2$O$_4$

Fig. 5.2 XRD pattern of Ni $_{0.2}$Cd $_{0.8}$Fe$_2$O$_4$. In lattice parameter calculation both Cu-Kα_1 and Cu-Kα_2 lines were considered.
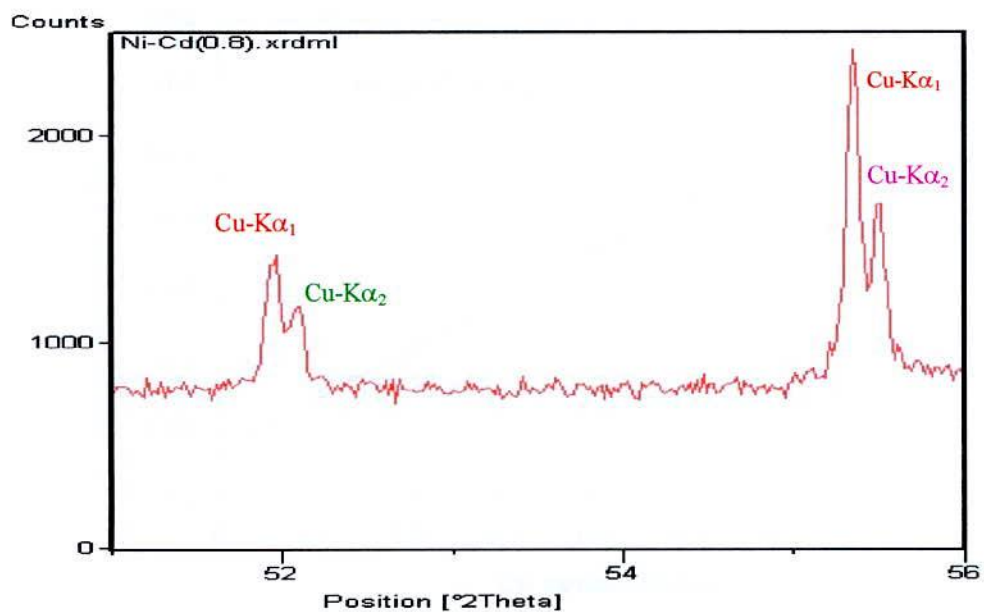
Fig. 5.3 Expanded form of Fig. 5.2 of 2θ range from $51°$ to $56°$ with clear identification of Cu-Kα_1 and Cu-Kα_2 lines.
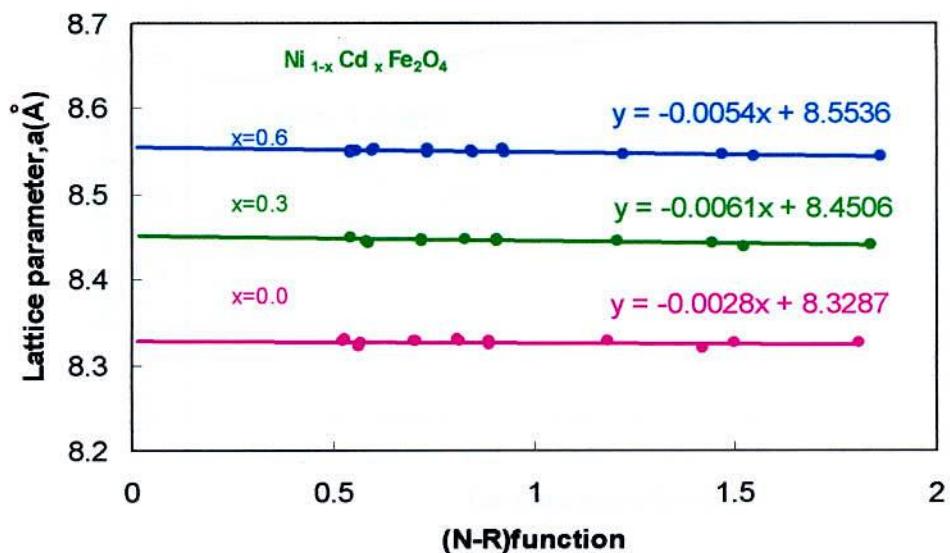
Fig.5.4: Lattice parameter a, vs (N-R) function plots of different compositions of $Ni_{1-x}Cd_xFe_2O_4$ from which a_0 has been determined.

It is observed that the X-ray density increases linearly with the increase of Cd concentration. The bulk density increases faster at x = 0.2 and thereafter increases almost linearly. The result signifies that Cd has a pronounced effect on the densification of the $NiFe_2O_4$ when it is substituted by cadmium. Therefore it is expected that the $NiFe_2O_4$ ferrites, substituted by Cadmium, would give higher permeability according to the ref [7]. It is known that the porosity of ceramic samples results from the two sources, intra-granular porosity and intergranular porosity [13]. Thus the total porosity could be written as

$$P = P_{intra} + P_{inter} \qquad (5.2)$$

The intra-granular porosity mainly depends on the grain size [14]. The porosity of the investigated sample has been determined from the X-ray density and the measured bulk density using equation (4.6) and demonstrated in Table-2. It is understood from the data that the porosity decreases monotonically with the increase of Cd content, which further demonstrates that Cd has the beneficial effect on the densification of Cd substituted Ni ferrites.

5.2 Curie Temperature (T_c) Measurement

Curie temperature T_c is a basic quantity in the study of magnetic materials. It corresponds to the temperature at which a magnetically ordered material becomes magnetically disordered, i,e, becomes paramagnet. Curie temperature also signifies the strength of the exchange interaction between the magnetic atoms. T_c of all the $Ni_{1-x}Cd_xFe_2O_4$ ferrite samples have been determined from the temperature dependence of initial permeability except for the sample with x=0.8, which is paramagnetic at room temperature. Fig.5.7 shows the

55

temperature dependence of permeability for the samples x=0.0 to 0.6. T_c has been taken as the temperature at which a sharp fall of permeability is observed. The sharpness of the fall of permeability indicates the homogeneity and the single phase of the studied sample, which have also been confirmed by X-ray diffraction by our previous XRD experiment.

Curie temperature, T_c of the sample with x = 0.8 has been determined from the temperature dependence of magnetization, M from 5K-340K using a SQUID magnetometer since it is paramagnetic at room temperature. T_c of this sample has been found to be 172K(-101°C). This is noteworthy that this sample shows some interesting magnetic ordering with temperature as dependent on applied magnetic field. Discussion on this interesting phenomenon on the basis of magnetic ordering as affected by applied magnetic field and temperature is followed. Fig.5.8 and Fig.5.9 show the temperature dependence of magnetization with an applied magnetic field of 5 Oe and 1 Tesla respectively. Magnetisation curve as a function of temperature, M vs T with H = 5 Oe does not show any sign of ferromagnetism; rather it demonstrates a feature of M vs T which corresponds well with the antiferromagnetic ordering. It is observed from Fig.5.8 that as the temperature decreases, M increases in a manner as manifested in a paramagnetic substance, passing through a maximum at a critical temperature of 39K and falls thereafter. This critical temperature of 39K for x=0.8 may be termed as antiferromagnetic transition temperature T_N. The sample is paramagnetic above T_N and antiferromagnetic below it. But when applied magnetic field, H=10000 **Oe** (1Tesla) was used to measure M vs T , a different scenario has been observed with the absence of maxima (peak) and the nature of the temperature dependence of magnetization resembles ferromagnetic. The ferromagnetic transition temperature, T_c is difficult to extract from this high field magnetization curve due to the smearing of inflexion

point by high field effect. Therefore dM/dT of the M vs T data has been taken and plotted as a function of temperature, T as depicted in Fig.5.10, where maxima at T = 172K may be taken as the T_c of the sample. This field induced effect signifies that the sample with x = 0.8 is basically antiferromagnet with T_N = 39K which undergoes field induced ferromagnetic ordering at T_c = 172K. This type of magnetic behaviour with temperature with high content of non-magnetic catoins such as Zn and Cd is generally observed in Ni, Li and Mg based ferrites [14]. It is known that $CdFe_2O_4$ and $ZnFe_2O_4$ are paramagnetic at room temperature and show antiferromagnetic behavior at very low temperature [15, 16].When these ferrites are substantially diluted with higher content of non-magnetic Zn^{2+} and Cd^{2+}, spin canting and spin frustration takes place giving rise to antiferromagnetic/anomalous behavior as a function of temperature.

Fig. 5.11 and Fig.5.12 show the real and imaginary part (magnetic loss component) of the complex permeability as dependent on temperature. At the Curie temperature, where complete spin disorder takes place, corresponds to maximum of imaginary part of the permeability and sharp fall of the real part of permeability towards zero. Therefore for accurate determination of Curie temperature, the maxima of imaginary part and the corresponding sharp fall of the real part of the permeability towards zero is very essential, simultaneously to determine T_C accurately . For all the samples, the Curie temperatures have been determined, following the above-mentioned principle as shown in Fig. 5.7, where the imaginary component of the permeability μ" has not been shown for the clarity of the graph.

The determined Curie temperatures for the entire range of composition $Ni_{1-x}Cd_xFe_2O_4$ are collected and demonstrated in Fig.5.13 as a function of Cd content, x. A linear dependence of

the Curie temperature, T_c with Cd content, x is observed. A linear least square fitting of the Curie temperature with x, gives an empirical relation for the whole $Ni_{1-x}Cd_xFe_2O_4$ system as follows:

$$T_c(x) = T_{c0} - 878.5\, x \qquad (5.3)$$

where T_{c0} is the Curie temperature of the pure Ni-ferrite and $T_c(x)$ corresponds to the Curie Temperature of any composition having Cd concentration, x. From this empirical relation Curie temperature of $NiFe_2O_4$ is found to be 626°C. Our experimental result is 590°C and the literature value is 587°C- 597°C [16, 17 and 18].

The linear decrease of T_c with increasing Cd content may be explained by modification of the A-B exchange interaction strength due to the change of the iron distribution between A and B sites when nonmagnetic Cd is substituted for Ni. The basic magnetic properties of $NiFe_2O_4$ system originate from Ni^{2+} ions only in the octahedral B-sites since Fe^{3+} ions are distributed equally in both the A and B-sites. The substituted Cd^{2+} preferentially occupies the tetrahedral A-site replacing an equal amount of Fe^{3+} to octahedral B-sites. In such a situation J_{AA} becomes weaker. Therefore decrease of T_c is due to the weakening of A-B exchange interaction and this weakening becomes more pronounced when more Cd^{2+} replaces more tetrahedral Fe^{3+} to octahedral B-sites.
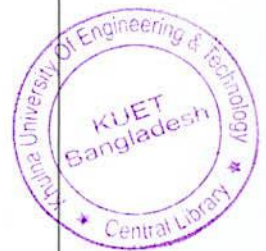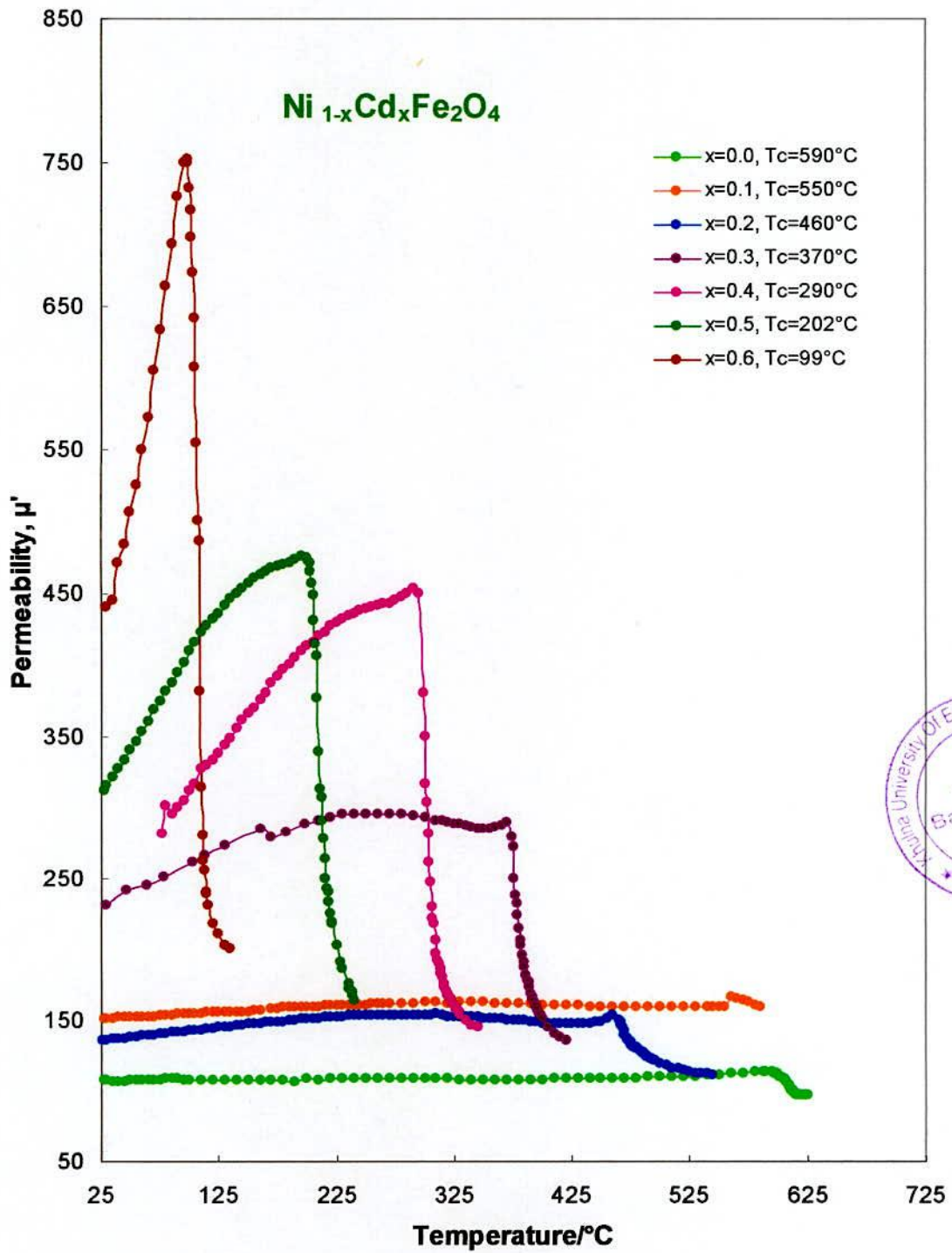
Fig.5.7. Permeability vs temperature for different compositions of $Ni_{1-x}Cd_xFe_2O_4$.
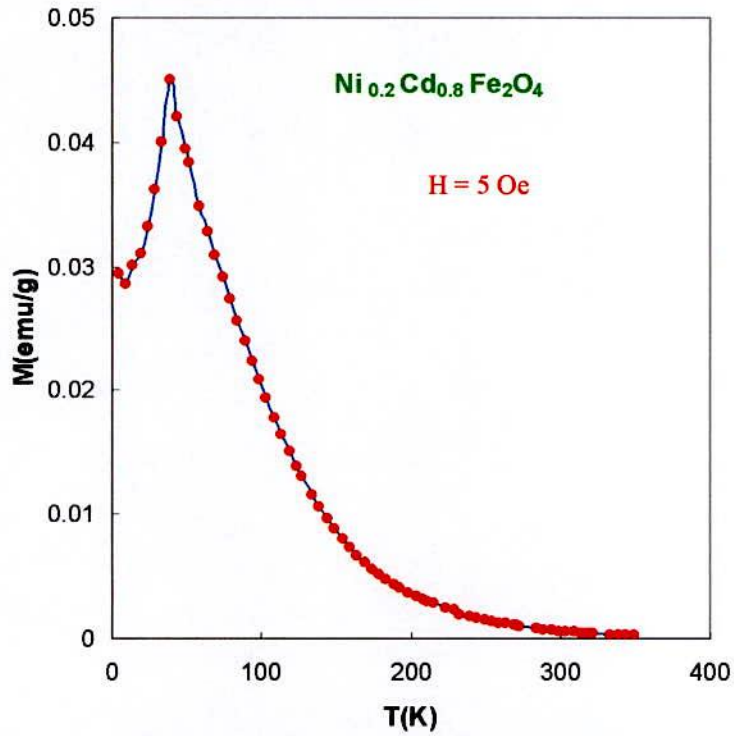
Fig. 5.8 Temperature dependence of low field magnetization
of $Ni_{0.2}Cd_{0.8}Fe_2O_4$ with an applied field of 5 Oe.
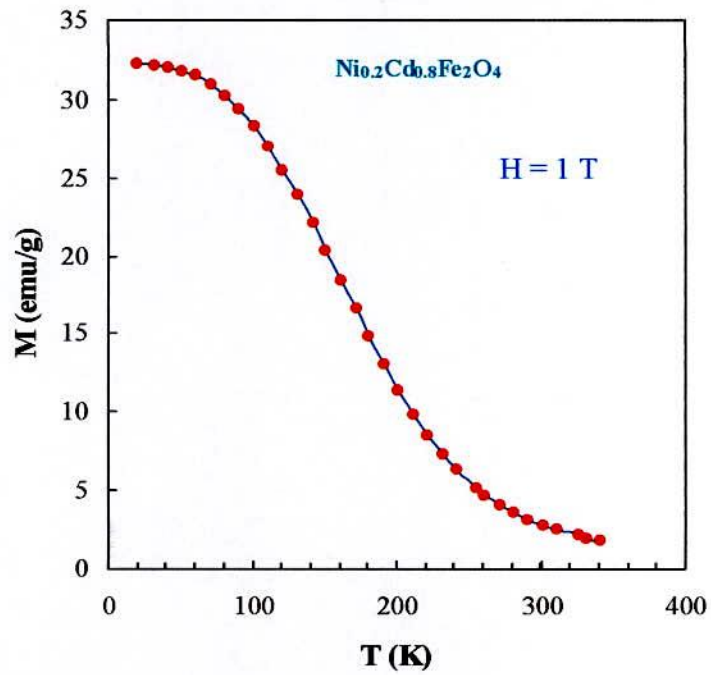
Fig.5.9 Temperature dependence of high field magnetization
with an applied field of 1T for $Ni_{0.2}Cd_{0.8}Fe_2O_4$.
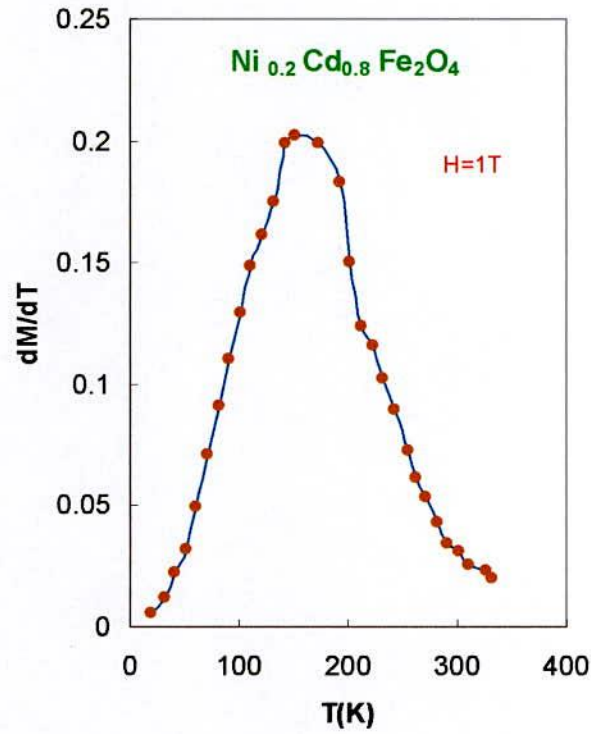
Fig. 5.10 Derivative of magnetization from the data of Fig.5.9 with respect to temperature(dM/dT), from which Curie temperature of Ni $_{0.2}$Cd$_{0.8}$Fe$_2$O$_4$ is determined.
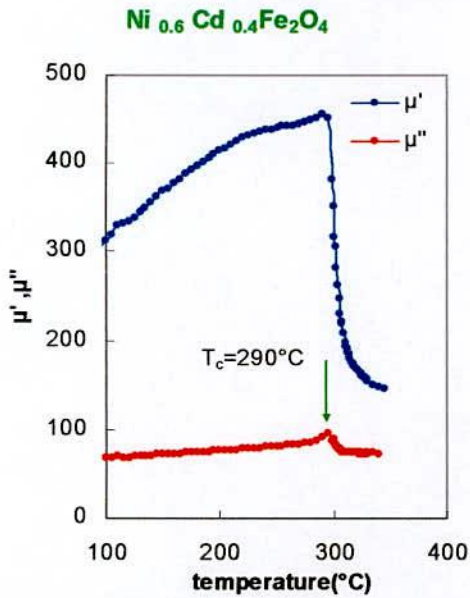
Fig. 5.11 Temperature dependence of the real and imaginary part of initial permeability of Ni $_{0.6}$Cd$_{0.4}$Fe$_2$O$_4$ sintered at 1200° C.
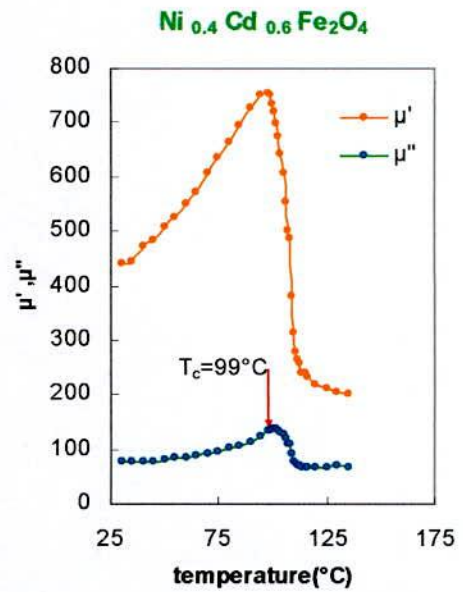
Fig. 5.12 Temperature dependence of the real and imaginary part initial permeability of Ni $_{0.4}$Cd$_{0.6}$ Fe$_2$O$_4$ sintered at 1200° C.

61
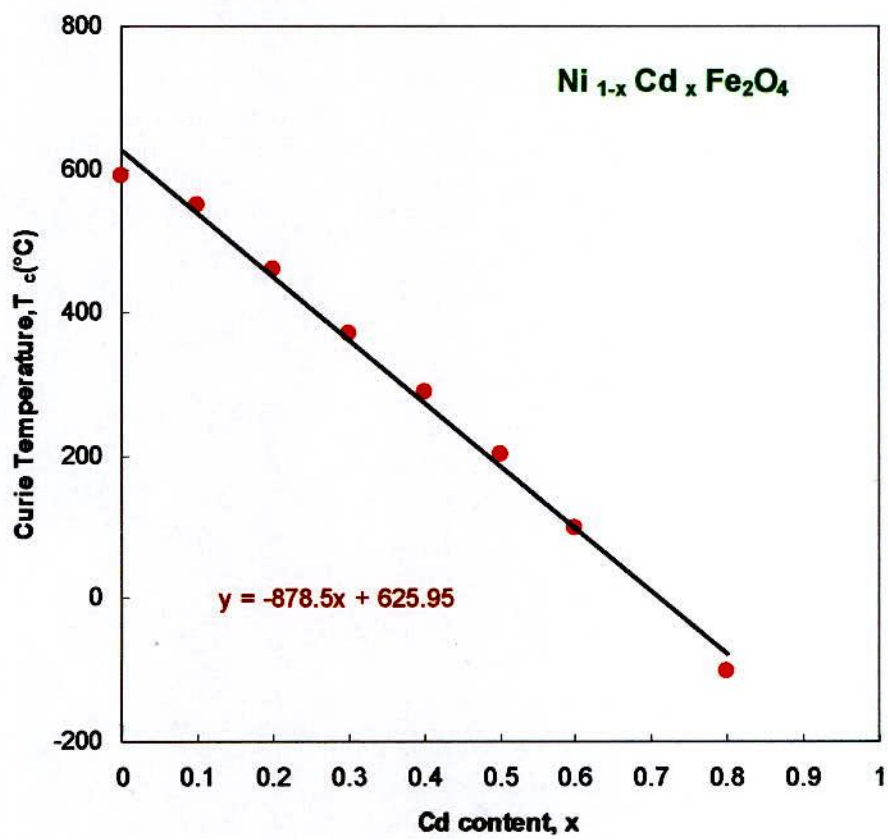
Fig.5.13. Varition of Curie Temperature (T_c) on Cd content.

5.3 Magnetization and Magnetic Structure of $Ni_{1-x}Cd_xFe_2O_4$

The magnetic ordering in the simple spinel ferrites is based on the Neel's two sub-lattices (tetrahedral A-site and octahedral B-site) model of ferri-magnetism in which the resultant magnetization is the difference between A-site and B-site magnetization, provided that they are co-linear and anti-parallel to each other, i.e.,

$$M = M_B - M_A \tag{5.4}$$

Magnetization as a function of field at 20K measured with a SQUID magnetometer is shown in Fig.15 while Fig.14 shows the same measured with a VSM at room temperature. The magnetization of all the samples are saturated except for $x = 0.8$. The sample with $x = 0.8$ shows monotonous increase of magnetization with increasing magnetic field with no sign of saturation.

It is observed that the saturation magnetization increases with the increase of Cd content initially and then decreases thereafter. The composition for $x = 0.8$ show paramagnetic behavior at room temperature. A theoretical calculation of magnetic moment in Bohr magneton of $Ni_{1-x}Cd_xFe_2O_4$ system is demonstrated in Table-3. The saturation magnetization value of a sample has been taken the magnetization at high field where M is independent of magnetic field. The magnetic moment in Bohr magneton has been calculated from the measured saturation magnetization value per unit mass using the formula:

$$n_B = \frac{M M_s}{N \mu_B} \tag{5.5}$$

The result of the saturation magnetization M_s, magnetic moment in Bohr magneton, n_B in μ_B at 20K and room temperature together with the theoretically calculated magnetic moment on

the basis of cation distribution of the Ni^{2+}, Cd^{2+} and Fe^{3+} in the A-site and B-site, are shown in Table-4.

Table-3: Calculation of Theoretical magnetic moment of Ni-Cd ferrites:

Cation	Ni^{2+}	Cd	Fe^{3+}
Magnetic moment	2.0 μ_B	0 μ_B	5.0 μ_B

Cadmium Content, x	$Ni_{1-x}Cd_xFe_2O_4$	Postulated Tetrahedral ions & their magnetic moments		Postulated Octahedral ions & their magnetic moments		Theoretical magnetic moment per molecule at 0K in μ_B
0.0	$NiFe_2O_4$	Fe 5.0 μ_B		Ni 2.0 μ_B	Fe 5.0 μ_B	2.0
0.1	$Ni_{0.9}Cd_{0.1}Fe_2O_4$	$Fe_{0.9}$ 4.5 μ_B	$Cd_{0.1}$ 0 μ_B	$Ni_{0.9}$ 1.8 μ_B	$Fe_{1.1}$ 5.5 μ_B	2.8
0.2	$Ni_{0.8}Cd_{0.2}Fe_2O_4$	$Fe_{0.8}$ 4.0 μ_B	$Cd_{0.2}$ 0 μ_B	$Ni_{0.8}$ 1.6 μ_B	$Fe_{1.2}$ 6.0 μ_B	3.6
0.3	$Ni_{0.7}Cd_{0.3}Fe_2O_4$	$Fe_{0.7}$ 3.5 μ_B	$Cd_{0.3}$ 0 μ_B	$Ni_{0.7}$ 1.4 μ_B	$Fe_{1.3}$ 6.5 μ_B	4.4
0.4	$Ni_{0.6}Cd_{0.4}Fe_2O_4$	$Fe_{0.6}$ 3.0 μ_B	$Cd_{0.4}$ 0 μ_B	$Ni_{0.6}$ 1.2 μ_B	$Fe_{1.4}$ 7.0 μ_B	5.2
0.5	$Ni_{0.5}Cd_{0.5}Fe_2O_4$	$Fe_{0.5}$ 2.5 μ_B	$Cd_{0.5}$ 0 μ_B	$Ni_{0.5}$ 1.0 μ_B	$Fe_{1.5}$ 7.5 μ_B	6.0
0.6	$Ni_{0.4}Cd_{0.6}Fe_2O_4$	$Fe_{0.4}$ 2.0 μ_B	$Cd_{0.6}$ 0 μ_B	$Ni_{0.4}$ 0.8 μ_B	$Fe_{1.6}$ 8.0 μ_B	6.8
0.8	$Ni_{0.2}Cd_{0.8}Fe_2O_4$	$Fe_{0.2}$ 1.0 μ_B	$Cd_{0.8}$ 0 μ_B	$Ni_{0.2}$ 0.4 μ_B	$Fe_{1.8}$ 9.0 μ_B	8.4
1.0	$CdFe_2O_4$	$Fe_{0.0}$ 0.0 μ_B	$Cd_{1.0}$ 0 μ_B	$Ni_{0.0}$ 0.0 μ_B	$Fe_{2.0}$ 10 μ_B	10.0

Table-4 : Saturation magnetization, Curie temperature and Magnetic moment for $Ni_{1-x}Cd_x Fe_2O_4$.

Cadmium content, x	Curie Temperature, T_c (°C)	Saturation magnetization at room temperature, M_s (emu/g)	Saturation magnetization at 20K M_s (emu/g)	Magnetic moment (μ_B) at room temperature	Magnetic moment (μ_B) at 20K	Theoretical Magnetic moment (μ_B) at 0K
0.0	590	48.4	51.2	2.04	2.15	2.0
0.1	550	69.1	69.1	2.97	2.97	2.8
0.2	460	73.7	85.5	3.23	3.75	3.6
0.3	370	76.5	95.5	3.43	4.26	4.4
0.4	290	71.2	103.2	3.26	4.73	5.2
0.5	202	54.4	102.7	2.54	4.81	6.0
0.6	99	39.3	93.4	1.88	4.46	6.8
0.8	-101	0.0	32.8	0.00	1.63	8.4

Note : Theoretical magnetic calculation in (μ_B) is shown in table-3 considering the preferred site occupancy of various cations according to neutron diffraction data.

Fig. 5.16 and Fig.5.17 shows the dependence of M_s and μ_B of the $Ni_{1-x}Cd_xFe_2O_4$ system measured at 20K and room temperature. It is observed that magnetization increases with Cd content up to x = 0.3 at room temperature and up to x = 0.5 at 20K. Above these concentration magnetization decreases sharply. The initial increase of magnetization is due to the dilution of magnetic moment of A-sublattice by substitution of nonmagnetic Cd ions. Since the resultant magnetization is the difference between the B and A sub-lattice magnetization as shown in equation 5.1, it is obvious that increase of net magnetization/magnetic moment is expected on dilution of the A-sublattice magnetization due to occupation of A-site by nonmagnetic Cd as well as enhancement of B-sublattice magnetization due to the introduction of Fe^{3+} ions having $5\mu_B$
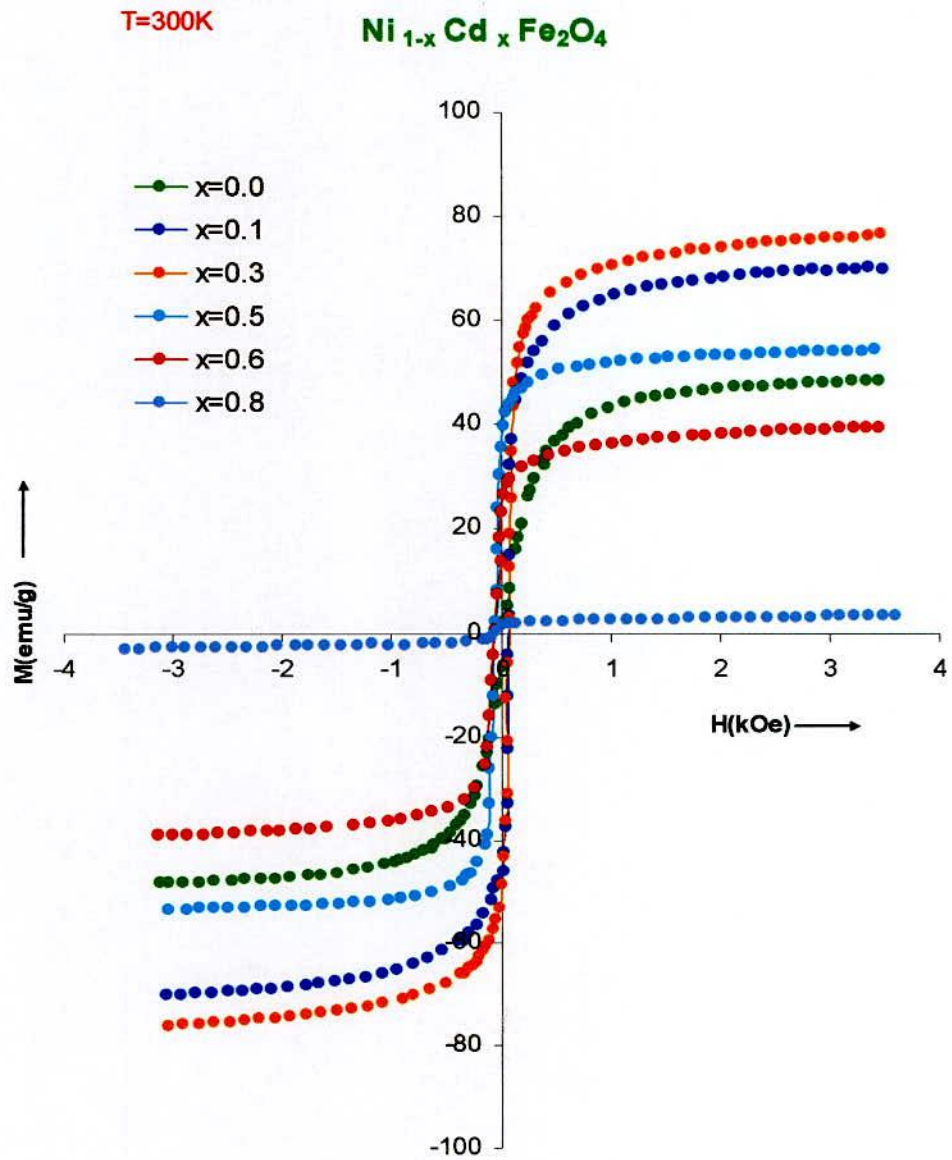
Fig.5.14 Magnetization curve measured at 300K as a function of field of Ni $_{1-x}$Cd $_x$Fe$_2$O$_4$ ferrites sintered at 1200°C for 4 hours.
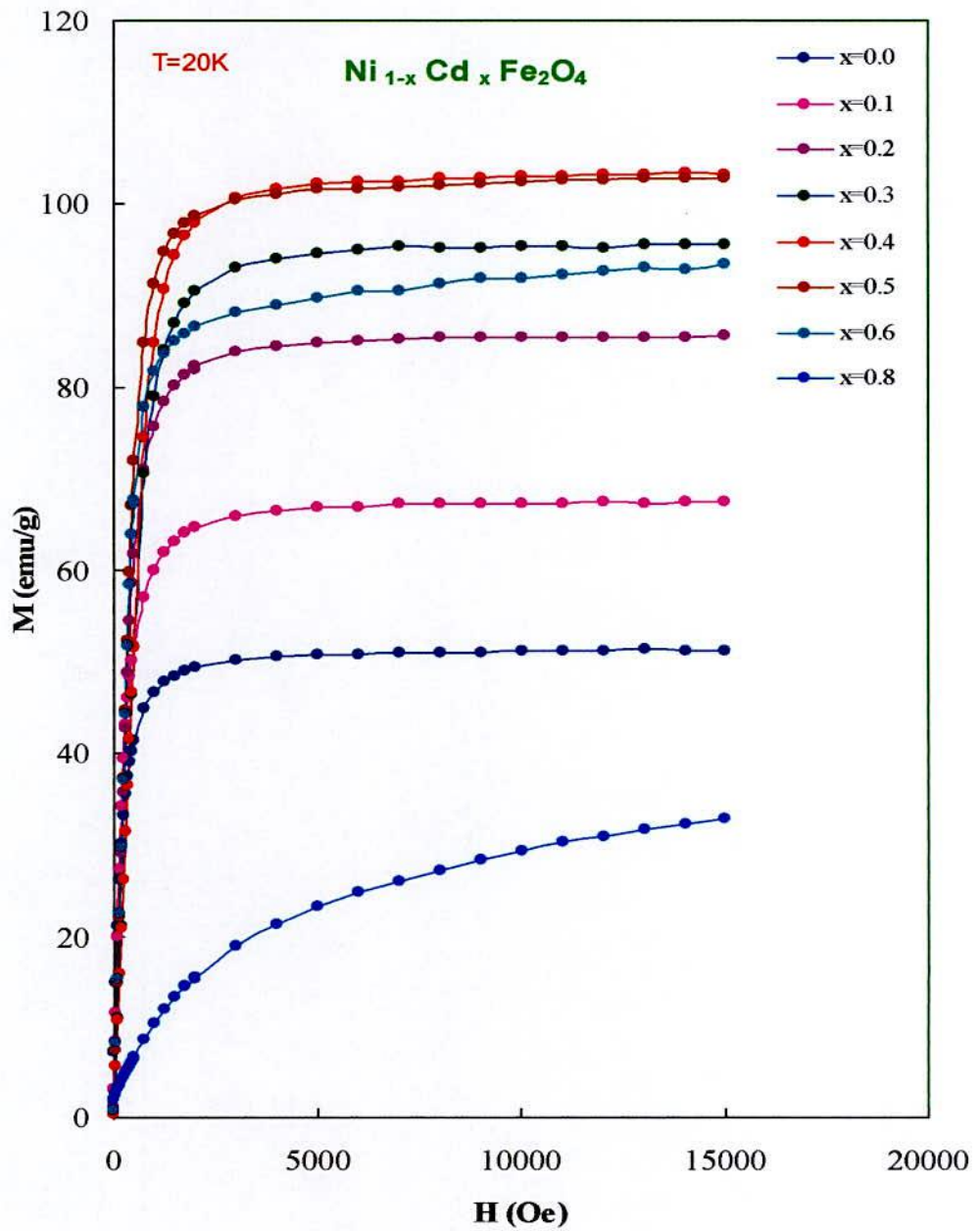
Fig. 5.15 Magnetization curve measured at 20K as a function of field of $Ni_{1-x}Cd_xFe_2O_4$ ferrites sintered at 1200°C for 4 hours.
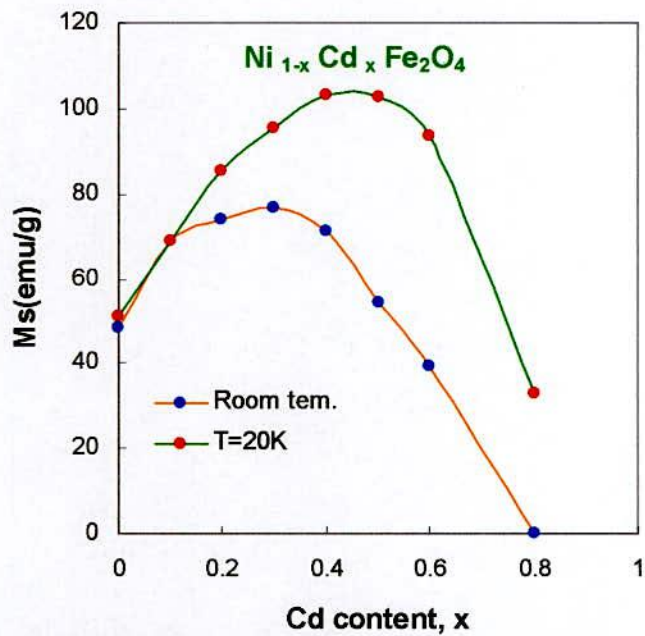
Fig.5.16 Saturation magnetization (M_s) of $Ni_{1-x}Cd_xFe_2O_4$ as a function of Cd content at room temperature and 20K .
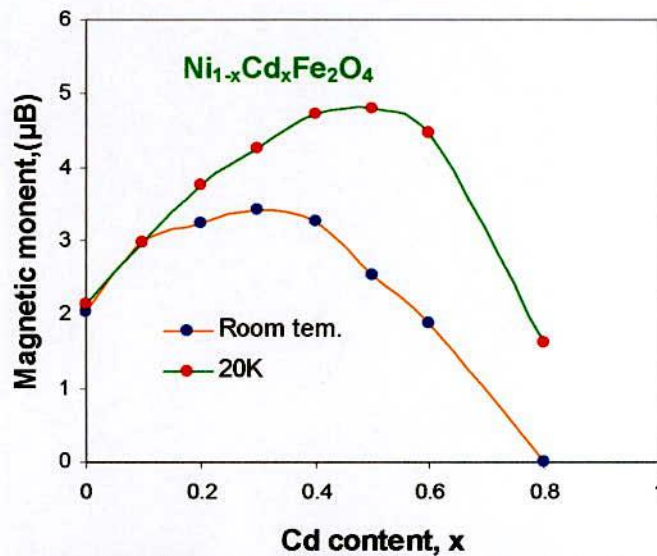
Fig.5.17 Magnetic moment in Bohr magneton (μ_B) of $Ni_{1-x}Cd_xFe_2O_4$ as a function of Cd content at room temperature and 20K.

moment. This initial rise of magnetization can be explained on the basis of Neel's two sublattice model.

The reason for decrease of magnetization beyond x = 0.3 at room temperature and x = 0.5 at 20K is that, beyond this limit the magnetization of A-sublattice is so much diluted that the A-B exchange interaction becomes weaker or comparable with the B-B exchange interactions. This disturbs the parallel arrangement of spin magnetic moments on B-site paving way for canted spins. Zn^{2+} and Cd^{2+} substituted ferrites have the tendency of manifestation of similar type of canting behavior above a certain limit of their contents [19, 20]. The existence of canted spin gives rise to Yafet- Kittel (Y-K) angle which compares the strength of A-B and B-B exchange interaction. Neel's two sublattice model is unable to explain the decrease of magnetization. The decrease of magnetization can be treated theoretically by triangular arrangement of spins as proposed by Yafet and Kittel (Y-K) [21]. The Y-K angles are found to increase with the increase of Cd content [19]. The physical origin of this spin arrangement is from the canting of the spins in the B-sublattice due to weakening of the intersublattice interaction J_{AB} and enhancing of intersublattice interaction J_{BB} on nonmagnetic Cd substitution in the A-sublattice. As in the case of spinels, J_{BB} is antiferromagnetic, the B-sublattice splits into two sublattices forming an angle (YK angle) between the directions of the spins resulting in a decrease of net B-sublattice magnetization. Satya Murthy et al from their neutron diffraction study on Ni-Zn system with high content of Zn have observed the occurrence of this noncolinear spin arrangements resulting in a sharp decrease of magnetization [22]. If the spin canting has not occurred with higher Cd content, the magnetic moment of the entire series would increase monotonically reaching a value of $10\mu_B$ for $CdFe_2O_4$ as shown in Table-3.

5.4 Permeability of $Ni_{1-x}Cd_xFe_2O_4$

Initial permeability as dependent on frequency and temperature of a magnetic material is an important parameter from the application consideration such as an insulator. Therefore the study of initial permeability/susceptibility has been a subject of great interest from both the theoretical and practical points of view. The optimization of the dynamic properties such as complex permeability in the high frequency range requires a precise knowledge of the magnetization mechanisms involved. The magnetization mechanisms contributing to the complex permeability, $\mu = \mu' - i\mu''$, in soft polycrystalline ferrites have been a controversial subject for a long time and remain unsolved satisfactorily. Although it is admitted that two mechanisms are involved in this phenomenon, the domain wall displacement and the spin rotation in the domains, the incertitude of the contributions from each of the mechanisms makes a theoretical interpretation of the experimental results rather difficult [23]. Complex permeability has been calculated as function of frequency, f upto 13 MHz at room temperature for all the samples of the series $Ni_{1-x}Cd_xFe_2O_4$ ferrites by using the conventional technique based on the determination of the complex impedance of a circuit loaded with toroid shaped sample. Fig. 5.18 to Fig. 5.21 represents the results of the real part of the permeability, μ' as a function of frequency for the whole series of ferrite samples sintered at 1100, 1150, 1200 and 1250^0C for 4 hours. We can call this real part of the permeability, μ' as initial permeability, μ' since the applied ac driving field is as low as 10^{-3} Oe and the independent nature of μ', i.e., $H_{ac} \to 0$, $f \to 0$, the criteria for the determination of initial permeability is fulfilled. It is clearly evident from these figures that with the increasing of Cd content, x the permeability μ' increases monotonically except for x =0.8. The sample with x=0.8 is paramagnetic at room temperature since its Curie temperature is found to be -101^0C as previously mentioned. Therefore its permeability should be zero. The small finite value of permeability as shown in Fig. 5.18 to 5.21 is an experimental artifact arising from the small applied field (10^{-3} Oe) that influences the magnetic domains to give rise to small magnetization and hence small value of μ' is observed. For all sintering temperatures initial permeability increases with the increase of x content.
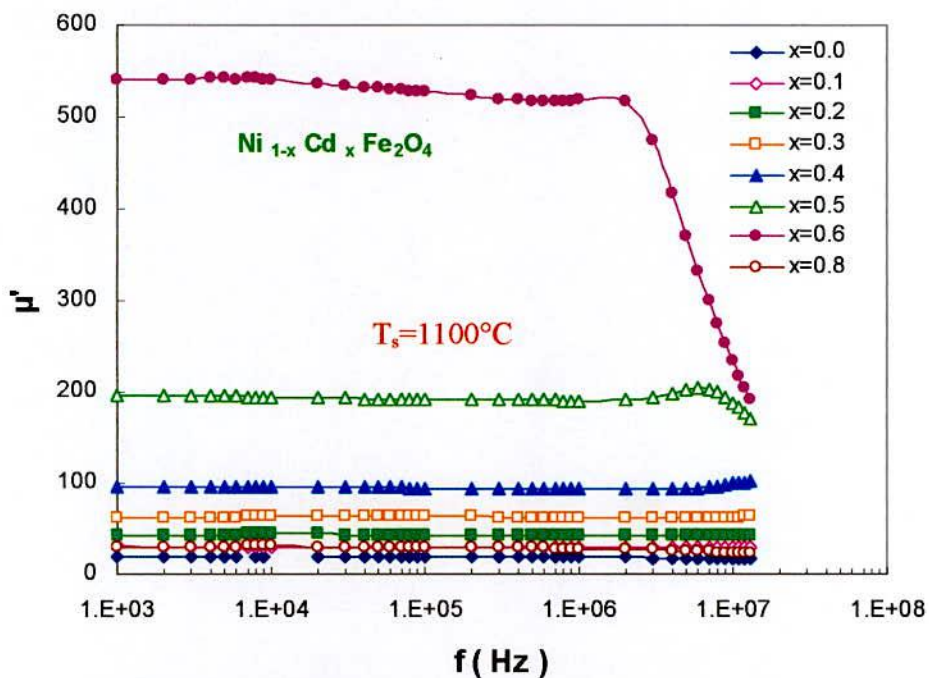
Fig. 5.18. Permeability (μ') vs frequency (f) of Ni $_{1-x}$ Cd $_x$ Fe$_2$O$_4$ sintered at 1100°C for 4 hours.
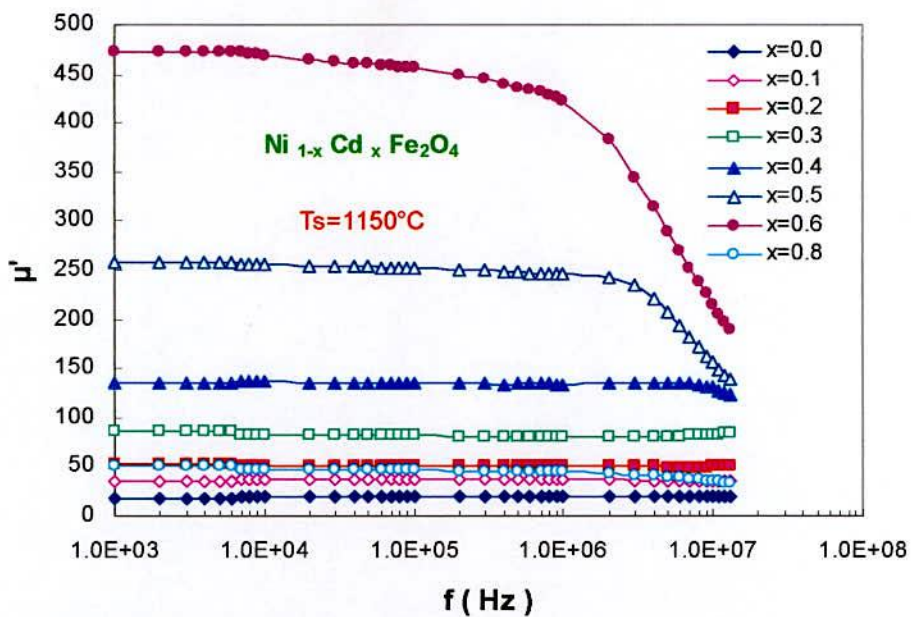
Fig. 5.19. Permeability (μ') vs frequency (f) of Ni $_{1-x}$ Cd $_x$ Fe$_2$O$_4$ sintered at 1150°C for 4 hours.

71
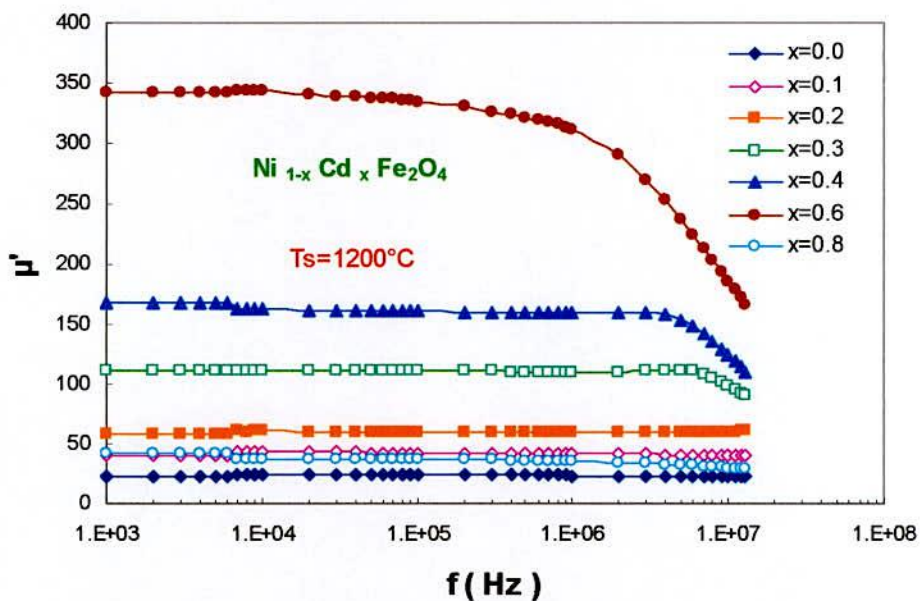
Fig. 5.20. Permeability (μ') vs frequency (f) of Ni $_{1-x}$ Cd $_x$ Fe$_2$O$_4$ sintered at 1200°C for 4 hours.
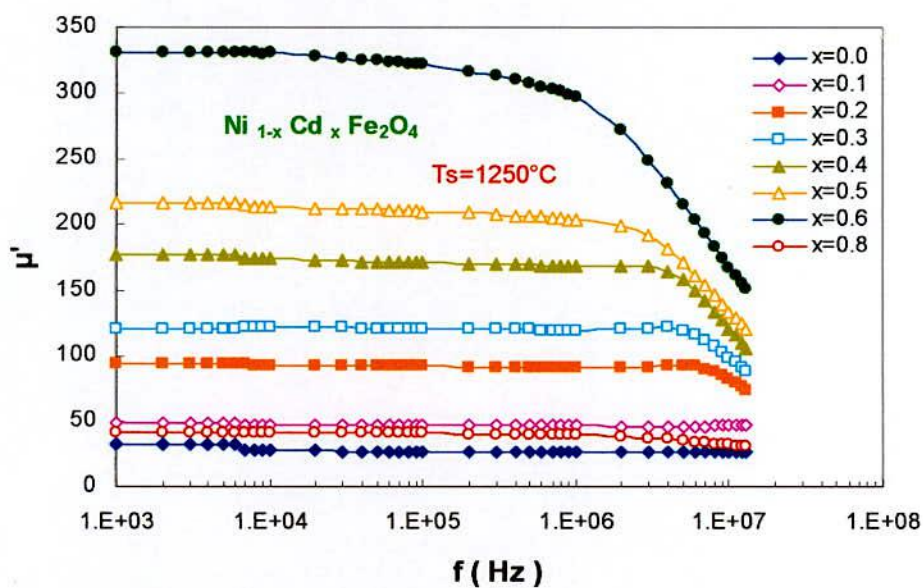
Fig. 5.21. Permeability (μ') vs frequency (f) of Ni $_{1-x}$ Cd $_x$ Fe$_2$O$_4$ sintered at 1250°C for 4 hours.
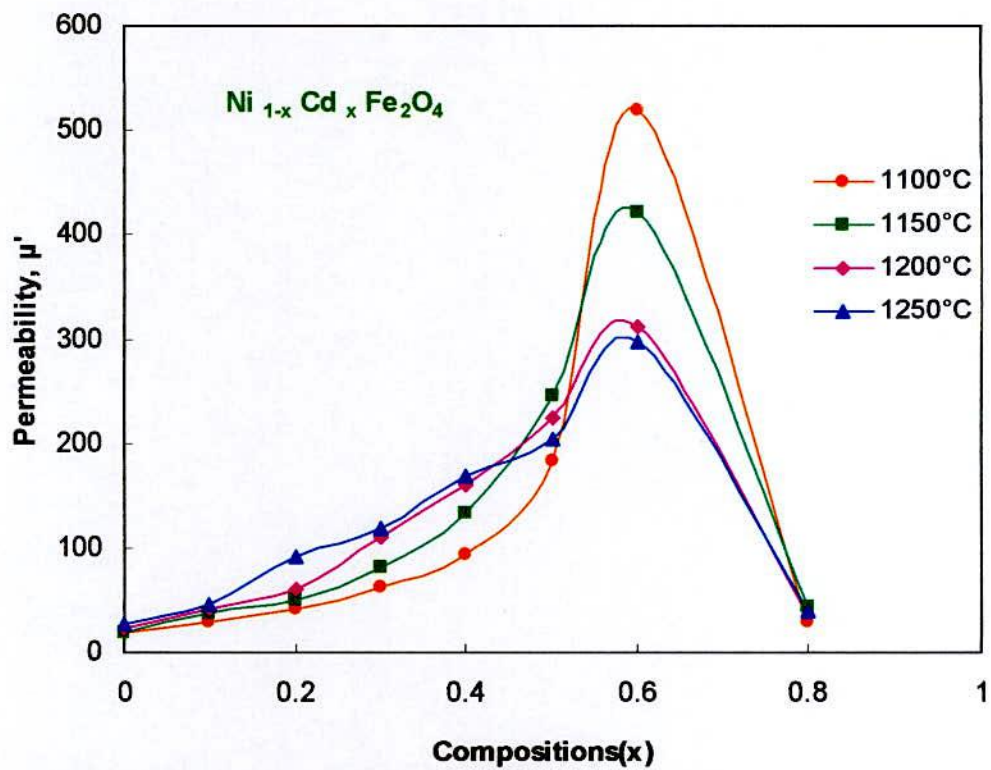
Fig. 5.22. Permeability (μ') vs compositions(x) of $Ni_{1-x}Cd_xFe_2O_4$ at 1MHz sintered at different temperatures for 4 hours.

Table-5: Real permeability and relative loss factor of $Ni_{1-x}Cd_xFe_2O_4$, sintered at different temperatures.

Cadmium content, x	T_s=1100°C		T_s=1250°C	
	Real permeability, μ'	Relative quality factor, μ'/D	Real permeability, μ'	Relative quality factor, μ'/D
0.0	18	339	26	697
0.1	29	777	46	1735
0.2	57	2628	91	2376
0.3	62	2696	119	2842
0.4	93	4635	168	2818
0.5	183	8805	204	2143
0.6	518	5189	297	1783
0.8	28	299	39	455

This is also true for a particular concentration of Cd content that the initial permeability similarly increases as the sintering temperature, T_S is increased. The exception is with the sample x = 0.6 and 0.5. For the sample with x = 0.6 the maximum initial permeability is observed at a sintering temperature of T_S =1100°C. As the T_S increases from 1100°C to 1250°C the permeability gradually decreases from 518 to 297 at 1 MHz. While for x = 0.5 permeability at T_S = 1100°C is 183 which increases to a maximum value of 245 at T_S = 1150°C and decreases thereafter attaining a value of 204 at T_S = 1250°C.The decrease of permeability with increasing T_s for samples x = 0.6 and 0.5 may be explained on the basis of intragranular pores entrapped within the grains which create constraint on the domain wall mobility. As a result initial permeability decreaes. At higher sintering temrerature pores cannot move so fast as compared with the grain growth. Therefore the pores cannot move to the grain boundary rather they are trapped within the grains. The results of μ'at 1 MHz for all the samples sintered at various temperatures are demonstrated in Fig.5.22 and Table-5 together with the relative quality factor, μ'/D which determines the merit of the magnetic materials from the application point of view. The optimum quality factor has been found with

74

the sample x = 0.5 sintered at T_S = 1100^{0}C to be 8805 as shown in Table-5. It is observed from the figures 5.18 to 5.21 that the stability of permeability against frequency is quite high. Permeability at T_S = 1100^{0}C is almost independent of frequency upto 13 MHz when Cd content is x ≤ 0.4, and it gradually decreases to lower frequency value as x increases above x = 0.4. For example sample with x = 0.6 at T_S =1100^{0}C μ' is independent of frequency up to f = 2 MHz. As the sintering temperature increases from 1100^{0}C to above, stability of μ' against f decreases to lower frequency value. However the stability of μ'-f up to 3 MHz for all the samples sintered even at 1250^{0}C except x = 0.6 is well manifested in the fig. 5.21. For high frequency application this property of μ'-f stability is an important criterion.

The permeability value for all the samples remains independent of frequency until resonance takes place, above which it starts decreasing sharply with simultaneous increase of imaginary part of the permeability. The resonance frequency, f_r corresponds to the maximum of the imaginary part of the permeability, μ'' where magnetic losses can be expressed as the ratio $\tan \delta = \dfrac{\mu''}{\mu'}$. From the study of complex permeability it has been revealed that the initial permeability increases with Cd content for all cases as well as with sintering temperature for all the samples except x = 0.5 and 0.6. Comparing the data of sintered bulk densities of all the samples sintered at T_S = 1200^{0}C which increases with Cd addition as shown in Table-2 and Fig. 5.6, it is understood that the increase of initial permeability with increasing Cd content is due to the densification and grain size of the samples. Grain size is expected to grow with the increase of sintering temperature and it has also been demonstrated that permeability increases with the increase of density [7]. Ferrites with higher density and larger average grain size posses a higher initial permeability. Nakamura [24] studied the magnetic properties of Ni-Zn-Cu ferrites and showed that sintering density and the average grain size increased with increasing sintering temperature. This is worth mentioning here that these changes are responsible for variations in magnetization, initial permeability and electrical resistivity.

The permeability can be expressed as μ = 1+χ_{spin} +χ_{dw}, where the χ_{spin} is the susceptibility due to the spin and χ_{dw} is the susceptibility due to the domain wall motion [24]. The dispersion of domain wall component depends on the square of the frequency and that of spin

rotational component is inversely proportional to the frequency. The domain wall motion contribution starts to decrease at lower frequency and the spin rotational component decreases at relatively higher frequencies [25].

Globus et al.[26] have developed an equation correlating static susceptibility (μ_s-1) and the resonance frequency , f_r corresponding to the maximum of the imaginary part of the complex permeability μ'' to saturation magnetization , M_s and grain diameter , D as given below :

$$(\mu_s - 1) = \frac{3M_s^2 \, 4\pi D}{16 E_w} \tag{5.6}$$

and
$$f_r = \frac{16 E_w}{\pi \beta D^2} \tag{5.7}$$

where E_w is the wall energy and $E_w = K\delta w$; where K is the anisotropy energy and δw is the domain wall thickness.

$$(\mu_s - 1)f_r = \frac{12}{\beta D} M_s^2 \tag{5.8}$$

where, β is the domain wall damping factor, $(\mu_s - 1)f_r$ is known as Snoek's product which is constant.

According to the Globus model, the relaxation frequency, the static permeability and their product are microstructure dependent. Large grain size leads to high permeability and low resonance frequency. The smaller the grain size, the higher the $(\mu_s - 1).f_r$ product up to a critical size for which the grains becomes mono-domain. On the contrary, Snoek's model is only related to spin rotations [27].

In this model, the static susceptibility (μ_s-1) and the resonance frequency f_r are given by:

$$(\mu_s - 1) = \frac{2M_S}{3H_a} \tag{5.9}$$

and
$$f_r = \frac{\gamma}{2\pi} H_a \tag{5.10}$$

where γ is the gyromagnetic ratio, H_a the anisotropy field and M_s the saturation magnetization. Thus :
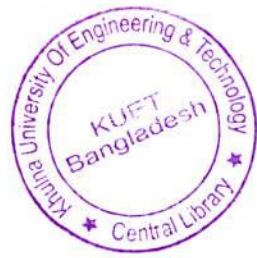
$$(\mu_s - 1)f_r = \frac{\gamma}{3\pi}M_s \tag{5.11}$$

The $(\mu_s - 1).f_r$ product depends only on saturation magnetization. So according to the model, grain size is not a relevant parameter for a polycrystalline ferrite. In our present study we would apply the model of Globus in which the permeability is directly proportional to the micro structural features i.e., grain size. As grain size increases, the multi domain grains are obtained which induces in higher permeability values due to the domain wall contribution [24, 26]. Also an increase in the density of ceramics not only results in the reduction of demagnetizing field due to reduction of pores but also raises the spin rotational contribution, which in turn increases the permeability [28]. From the observation of μ' - f spectra for all the samples as shown in Fig. 5.18 to Fig. 5.21 sintered between 1100°C to1250°C, dispersion of permeability, with frequency shifts to lower frequency range with the increase of Cd content resulting from higher permeability. Dispersion or resonance could not be observed in our studied samples with lesser content of Cd as well as sintered at lower temperature since our measurement facility could not be extended beyond 13 MHz. Again this increasing permeability with increasing Cd content is connected with increased density, grain size and possibly reduction of anisotropy energy with the addition of nonmagnetic Cd. Moreover as the sintering temperature increases dispersion of μ'-f also shifts to the lower frequency range as a result of increasing density and grain size, as proposed by Nakamura [24]. Therefore the increase in permeability, μ' and decrease of dispersion frequency or resonance frequency to lower frequency range with increasing Cd content and sintering temperature can be well explained on the basis of equations (5.6) and (5.8).

5.5 Resistivity

Resistivity is an important electrical property. Table -6 gives the dc resistivity values for all the samples under study. The highest value of resistivity is obtained for pure $NiFe_2O_4$. Resistivity decreases with the increase of Cd content as well as with increasing sintering temperature. From the Table it is also noticed that for the sample x = 0.6 and 0.8 sintered at

1200°C, an increase of resistivity is observed. This increase of resistivity may be attributed to the entrapped intragranular porosity, which has been manifested in our permeability result. Sankpal et al. [29] have measured resistivity as a function of composition in their work on Ni-Cu ferrite. They obtained the similar trend of decreasing resistivity with the increase of Cu content. This trend could be attributed to the high activation energy, which is associated with high resistivity at room temperature. When the polycrystalline ferrites are considered the bulk resistivity arises from a combination of the crystallite resistivity and the resistivity of the crystallite boundaries. The boundary resistivity is much greater than that of crystallite resistivity. So the boundaries have the greatest influence on the DC resistivity [30]. The decrease of resistivity has been related to the decrease of porosity at higher sintering temperatures since pores are non-conductive, which increases the resistivity of the material [31]. The resistivity decreases with decreasing porosity because the charge carriers on their way face less number of pores. But in spite of high density and less porosity if very small fraction of intragranular porosity exists in a ferrite material, which may be observed when the sintering kinetic is very fast, the resistivity might increase as has been evidenced in our studied sample of $x = 0.6$ and 0.8.

Table- 6: Room temperature resistivity for $Ni_{1-x}Cd_xFe_2O_4$ sintered at different temperatures for 4 hours.

Cadmium content, x	Resistivity ρ (Ω.cm) $T_s= 1100°C$	Resistivity ρ (Ω.cm) $T_s= 1150°C$	Resistivity ρ (Ω.cm) $T_s= 1200°C$
0.0	5.72×10^7	1.71×10^7	-
0.1	3.34×10^7	1.31×10^7	3.19×10^6
0.2	1.82×10^7	-	4.6×10^3
0.3	-	5.6×10^6	1.5×10^3
0.4	3.5×10^6	3.4×10^6	1.8×10^3
0.5	1.57×10^4	1.45×10^4	1.3×10^3
0.6	8.6×10^3	8.4×10^3	2.83×10^3
0.8	8.5×10^3	8.6×10^3	4.6×10^3

References:

[1] V. A. M. Brabers and J.K.J. de physique **4**(1977)207.

[2] L. Vegard , Z. Phys., **5**(1921) 17.

[3] JMMM **223**(2001) 127.

[4] G. Blasse, Philips Res. RE=ep. Suppl. **3**(1964)91.

[5] A. Globus , H. Pascard and V. Cagan, J. de Physique **38,C1**(1977) 138.

[6] N. Reslescu , L. Sahelarie, L. Rezlescu and P.D. Popa, Cryst. Res. Tech. **36**(2001)157.

[7] J. Smit, H. P. J. Wign, Ferrites, Wiley, New York 1959(144-252).

[8] Satya Murthy, N. S. , M. G. Natera, R. J. Begum and SI Youssef, in. Proc. 1st Int. Conf. Ferrites, Tokyo,(1970)60.

[9] Gorter , E. W. , Philips Res. Rep. **9**(1954)295.

[10] Fissov, Y.P. and G. P. Popov, Zh. Fiz. Khim **55**(1981)603.

[11] OteroArean, C., E. Garcia Diaz, J. M. Rubio Gonzalez and M. A. Villa Garcia, J. Solid State Chem. **77**(1988)275.

[12] P. N. Vasambekar, C. B. Kolebar, As. Vaingankar, J. Magn. Magn. Mat. **186**(1998)333.

[13] A. A. Sattar, H. M. El-Sayed, K. M. El-Shokrofy and M. M. El-Tabey, " Improvement of the magnetic properties of Mn- Ni- Zn ferrite by the non magnetic Al^{3+} ion substitution", J. Appl. Sci. **5(1)**(2005) 162.

[14] S. S. Belled, S C Watawe, A M Shaikh and B K Chougule. Bull. Mater. Ind. Acad. Sci.,**23**(2000).

[15] Tellefsen, M., L. Carreiro, R. Kershaw, K. Dwight and A. World J. Phys. Chem. Solids **88**(1984)754.

[16] B. D. Cullity, Introduction to Magnetic Materials. Addison- Wesley Pub. Com. (1972)188.

[17] Sawatzki, G. A., F. Van der Woude and A. H. Morrish,Phys. Rev. **187**(1967)747.

[18] Abe, M., M. Kaawachi and S. Nomura, J. Phys. Soc. Jpn **31**(1971)940.

[19] B. R. Karche, B. V. Khasbardar, A. S. Vaingankar, Journal of Mag. and Magnetic Materials **168**(1997)292-298.

[20] F. U. Ahmed, S. M. Yunus , I. Kamal, T. K. Datta, A. K. Azad, M. A. Hakim and M. A. Asgar , Nuclear Science and Appl. **7(1,2)**(1998)7-15.

[21] Y. Yafet and C. Kittel , Phys. Rev. **87**(1952)239.

[22] N. S. Satya Murthy, M. G. Natera, S. I. Youssef, R. J. Begum and C. M. Srivastava, Phys. Rev. **181**(1969)969.

[23] R. Lebourgeois, C. Le Fur , M. Labeyrie, M. Pate, J. P. Ganne, J. Magn. Magn. Materials **160**(1996)329.

[24] T. Nakamura, J. Magn. Magn. Mater. **168** (1997)265.

[25] O. F. Caltun, L. Spinu, Al. Stancu, L. D. Thung, W. Zhou, J. Magn. Magn. Mateer. **242-245** (2002) 160-162.

[26] A. Globus and P. Duplex, IEEE Trans. Mang. Mag-2 No. **3** (1966) 441-445.

[27] J. L. Snoek, Physica **14**(1948)202.

[28] J. J. Shrotri, S. D. Kulkarni, C. E. Deshpande, S. K. Date, Mater. Chem. Phys. **59**(1999)1.

[29] A. M. Sankpal, S. R. Sawant, A. S. Vaingankar, I. J. Pure, Appl. Phys. 26(1988)459.

[30] R. Narayan, R. B. Tripatri and B. K. Das – Pro. Of 5th Int.Conf. on ferrite. New Delhi(1989)267-273.

[31] M. A. El Hiti, J. Magn. Magn. Mater. **136**(1994)138.

CHAPTER VI

Conclusions

Conclusions

Among the soft ferrites Ni-Zn, Mg-Zn and Mn- Zn ferrites have enormous technological applications and accordingly extensive research have been carried out. It is well known that Mn-Zn ferrites have low resistivity and high saturation induction as compared with Ni-Zn and Mg-Zn ferrites and therefore it is used in lower frequency range. Ni-Cd ferrites are least studied. Zn and Cd both are paramagnetic but ionic radius of Cd^{2+} (0.97Å) is larger than that of Zn^{2+}(0.83 Å). So substitution of Cd in Ni_{1-x} Cd_x Fe_2O_4 may show some interesting properties since Cd^{2+} with larger ionic radius causes some lattice distortions. In this thesis work a detail investigation of Ni_{1-x} Cd_x Fe_2O_4 ferrites has been carried out to evaluate the structural, magnetic, electrical and physical properties.

A series of polycrystalline samples with the stoichiometric composition having the general formula Ni_{1-x} Cd_x Fe_2O_4 where x = 0.0 - 0.8, in step of 0.1, have been prepared using conventional double sintering ceramic method, sintered at 1100°C, 1150°C, 1200°C and 1250°C for 4 hours. The samples are characterized by X-ray Diffraction which confirms the single phase cubic spinel structure since no ambigious reflections other than the spinel structures are evidenced. For the precise determination of the lattice parameter, 'a' at higher angle reflections as well as wavelength corresponding to Cu-Kα_1 and Cu-Kα_2 are taken into consideration since they have different wavelengths. From the experimental results it is observed that the lattice parameter increases linearly with increasing Cd concentration obeying Vegard's law. This is attributed to the replacement of smaller Fe^{3+} ions (0.64 Å) from A-sites to B-sites by larger Cd^{2+} (0.97 Å). Bulk density increases monotonically with increasing Cd content signifying that Cd has a pronounced effect on the densification of the ferrites. The lattice parameter of Ni Fe_2O_4 is 8.3344Å and that of Cd Fe_2O_4 is 8.7009Å. These values have good coincidence with that of the standard values i.e., 8.34Å for Ni Fe_2O_4 and 8.70Å for Cd Fe_2O_4 respectively.

Curie temperature for pure Ni Fe_2O_4 is found to be 590°C which is a good matching with the literature value of 587-597°C. Curie temperature decreases linearly with increasing Cd content. This is due to the weakening of A-B exchange interaction.

Magnetic properties such as magnetization, permeability have been measured as a function of field, temperature and frequency, using vibrating sample magnetometer, SQUID magnetometer and Impedance Analyzer.

Magnetization as a function of field at 20K has been measured with a SQUID magnetometer shows the same measured with a VSM at room temperature. The magnetization of all the samples are saturated except for $x = 0.8$. The sample with $x = 0.8$ shows monotonous increase of magnetization with increasing magnetic field with no sign of saturation. It is observed that the saturated magnetization increases with the increase of Cd content initially and then decreases thereafter. The composition for $x = 0.8$ show paramagnetic behaviour at room temperature. The saturation magnetization increases with Cd content up to $x = 0.3$ at room temperature and up to $x = 0.5$ at 20K. Above these concentration magnetization decreases sharply. The initial increase of magnetization is due to the dilution of magnetic moment of A-sublattice by substitution of nonmagnetic Cd ions. Neel's two sublattice collinear model is applied for the initial rise of the magnetization up to $x \leq 0.5$, at 20K and beyond that three sublattice noncollinear model proposed by Yafet-Kittel are predominant. This suggests the existing of canted spin structure in the ferrite system with higher content of Cd.

Permeability increases with increasing Cd concentration as well as increasing sintering temperature for all the studied samples. From the observation of μ' - f spectra for all the samples sintered between 1100°C to1250°C, dispersion of permeability , with frequency shifts to lower frequency range with the increase of Cd content resulting from higher permeability . Dispersion or resonance could not be observed in our studied samples with lesser content of Cd as well as sintered at lower temperature since our measurement facility could not be extended beyond 13 MHz. Again this increasing permeability with increasing Cd content is connected with increased density, grain size and possibly reduction of anisotropy energy with the addition of nonmagnetic Cd. Moreover as the sintering temperature increases dispersion of μ' - f also shifts to the lower frequency range as a result of increasing density and grain size. For the sample with $x = 0.6$, the permeability decreases with increasing sintering temperature in spite of high density which may be attributed to the intragranular porosity that inhibits easy domain wall mobility resulting in a decrease of permeability.

The highest value of resistivity is obtained for pure $NiFe_2O_4$. Resistivity decreases with the increase of Cd content. The decrease of resistivity may be related to the decrease of porosity. Room temperature DC resistivity decreases with Cd content and sintering temperature.

Appendix

Table 7.1 : XRD data at different crystallographic plane (h k l).

x	Position(2θ)°	indexing plane h k l	d-spacing (Å)	lattice parameter,a (Å)
	30.37	220	2.9432	8.325
	35.77	311	2.5101	8.325
	37.45	222	2.4014	8.319
	43.46	400	2.0822	8.329
	53.89	422	1.7000	8.328
	54.06	422	1.6992	8.324
	57.46	511	1.6026	8.327
	57.60	511	1.6029	8.329
0.0	63.11	440	1.4720	8.327
	63.27	440	1.4722	8.328
	71.63	620	1.3163	8.325
	72.05	620	1.3158	8.322
	74.66	533	1.2702	8.329
	74.89	533	1.2700	8.328
	30.25	220	2.9547	8.357
	35.63	311	2.5199	8.358
	37.28	222	2.4122	8.356
	43.30	400	2.0898	8.359
	53.66	422	1.7067	8.361
	53.77	422	1.7077	8.366
	57.20	511	1.6090	8.361
	57.32	511	1.6098	8.365
	62.82	440	1.4781	8.361
0.1	62.93	440	1.4793	8.368
	71.24	620	1.3226	8.365
	71.40	620	1.3233	8.369
	74.30	533	1.2756	8.365
	74.51	533	1.2756	8.365
	75.26	622	1.2616	8.369
	75.52	622	1.2610	8.365
	30.10	220	2.9687	8.397
	35.44	311	2.5326	8.400
	37.07	222	2.4249	8.400
	43.10	400	2.0987	8.395
	53.38	422	1.7148	8.401
	53.57	422	1.7136	8.395
	56.89	511	1.6172	8.403
	57.02	511	1.6177	8.406
0.2	62.46	440	1.4857	8.404
	62.63	440	1.4857	8.404
	70.88	620	1.3284	8.402
	71.05	620	1.3289	8.405
	73.87	533	1.2818	8.405
	74.12	533	1.2813	8.402

Continuation of Table 7.1.

x	Position(2θ)°	indexing plane h k l	d-spacing (Å)	lattice parameter,a (Å)
	29.94	220	2.5441	8.441
	35.28	311	2.4370	8.438
	36.88	222	2.1110	8.442
	42.84	400	1.7237	8.444
	53.09	422	1.7242	8.444
	53.21	422	1.6254	8.447
	56.58	511	1.6256	8.446
	56.72	511	1.4929	8.447
0.3	62.12	440	1.4933	8.445
	62.28	440	1.3350	8.447
	70.48	620	1.3351	8.443
	70.67	620	1.2886	8.444
	73.42	533	1.2885	8.450
	73.64	533	2.9947	8.449
	29.84	220	2.5551	8.470
	35.12	311	2.4441	8.474
	36.77	222	1.7302	8.467
	52.87	400	1.7303	8.476
	53.01	422	1.6314	8.477
	56.35	511	1.6317	8.477
	56.49	511	1.4990	8.479
	61.84	440	1.4990	8.480
0.4	62.01	440	1.3408	8.480
	70.13	620	1.3417	8.480
	70.28	620	1.2931	8.486
	73.12	533	1.2932	8.479
	73.33	533	1.2787	8.480
	74.08	622	1.2779	8.482
	74.35	622	4.9057	8.477
	18.08	111	3.0065	8.497
	29.72	220	2.5645	8.504
	34.99	311	2.4539	8.505
	36.62	222	2.1276	8.501
	42.49	400	1.7380	8.510
	52.62	422	1.7379	8.514
	52.76	422	1.6381	8.514
	56.10	511	1.6388	8.512
0.5	56.22	511	1.5051	8.515
	61.57	440	1.5054	8.514
	61.72	440	1.3463	8.516
	69.80	620	1.3469	8.515
	69.97	533	1.2988	8.519
	72.75	533	3.0206	8.517

Continuation of Table 7.1.

x	Position(2θ)°	indexing plane h k l	d-spacing (Å)	lattice parameter,a (Å)
	29.57	220	2.5761	8.544
	34.83	311	2.4671	8.544
	36.42	222	2.1367	8.546
	42.30	400	1.7447	8.547
	52.40	422	1.7456	8.547
	52.51	422	1.6451	8.552
	55.84	511	1.6455	8.548
	55.98	511	1.5110	8.550
	61.30	440	1.5118	8.548
0.6	61.43	440	1.3522	8.552
	69.45	620	1.3519	8.552
	69.66	620	1.3039	8.550
	72.42	533	1.3040	8.550
	72.62	533	1.2889	8.551
	73.40	622	1.2888	8.550
	73.62	622	3.0432	8.549
	29.35	220	2.5974	8.607
	34.53	311	2.1529	8.615
	41.93	400	1.7585	8.612
	51.96	422	1.7591	8.615
	52.08	422	1.6585	8.618
	55.35	422	1.6586	8.618
	55.50	511	1.5235	8.618
	60.74	511	1.5235	8.618
	60.91	440	1.3627	8.618
X=0.8	68.84	440	1.3625	8.618
	69.05	620	1.3140	8.617
	71.78	620	1.3143	8.616
	71.97	533	1.2990	8.618
	72.74	533	1.2993	8.617
	72.93	622	2.5761	8.619

Monochromatic Cu radiation was used in the measurement, where
$Cu(K\alpha_1) = 1.540598$, $Cu(K\alpha_2) = 1.544426$ and $Cu(K\alpha_{avg}) = 1.541874$.

Table 7.2 : Frequency dependence of real part of the permiability (μ') of Ni$_{1-x}$Cd$_x$Fe$_2$O$_4$ at the room temperature sintered at T$_s$=1100°C for 4 hours.

Frequency in kHz	x=0.0	x=0.1	x=0.2	x=0.3	x=0.4	x=0.5	x=0.6	x=0.8
1	18.44	38.47	64.68	62.52	95.26	188.19	559.36	29.90
2	18.44	35.68	56.60	62.52	95.26	188.19	550.19	29.90
3	18.44	35.68	56.60	62.52	95.26	188.19	541.02	29.90
4	18.44	35.68	56.60	62.52	95.26	188.19	541.94	29.90
5	18.44	35.68	56.60	62.52	95.26	188.19	541.94	29.90
6	18.44	35.68	56.60	62.52	95.26	188.19	541.02	29.90
7	19.25	30.07	58.21	63.56	95.26	187.33	541.94	30.90
8	18.44	30.07	58.21	63.56	95.26	187.33	541.94	30.90
9	18.44	30.07	58.21	63.56	95.26	187.33	541.02	30.90
10	19.25	30.07	58.21	63.56	95.26	187.33	540.11	30.90
20	18.44	30.07	58.21	63.56	95.26	186.48	536.44	29.90
30	18.44	30.07	58.21	63.56	95.26	186.48	534.61	29.90
40	18.44	30.07	58.21	63.56	95.26	185.62	532.77	29.90
50	18.44	30.07	58.21	63.56	95.26	185.62	530.94	29.90
60	18.44	30.07	57.40	63.56	95.26	185.62	530.02	29.90
70	18.52	29.89	57.73	63.04	94.74	185.62	529.84	29.80
80	18.52	29.89	57.65	62.94	94.65	185.62	528.46	29.70
90	18.52	29.89	57.65	62.94	94.56	185.62	527.73	29.70
100	18.52	29.89	57.65	62.94	94.56	185.19	526.99	29.70
200	18.52	29.89	57.49	62.83	94.13	184.59	522.87	29.40
300	18.52	29.80	57.40	62.73	93.96	184.25	520.12	29.20
400	18.44	29.80	57.32	62.63	93.78	183.91	518.10	29.10
500	18.44	29.80	57.24	62.52	93.61	183.74	517.18	29.00
600	18.44	29.71	57.16	62.52	93.52	183.48	517.18	28.80
700	18.44	29.70	57.40	62.42	93.42	183.31	516.63	28.71
800	18.36	29.68	57.14	62.38	93.33	183.22	517.18	28.63
900	18.36	29.64	57.10	62.32	93.26	183.14	517.73	28.52
1000	18.32	29.62	57.02	62.28	93.18	183.14	518.38	28.42
2000	18.13	29.39	56.74	61.97	92.75	183.82	517.37	27.57
3000	18.03	29.26	56.60	61.82	92.83	186.56	474.82	26.83
4000	17.96	29.18	56.60	61.79	93.00	190.84	417.96	26.16
5000	17.91	29.13	56.60	61.79	93.52	195.29	370.46	25.56
6000	17.87	29.08	56.60	61.79	94.22	197.60	331.95	25.01
7000	17.84	29.05	56.72	61.90	95.20	196.65	300.50	24.52
8000	17.81	29.03	56.85	62.02	96.37	193.06	274.55	24.09
9000	17.79	29.01	57.02	62.17	97.71	188.02	252.63	23.71
10000	17.77	29.00	57.23	62.38	99.01	182.45	234.02	23.38
11000	17.75	28.99	57.47	62.62	100.11	176.81	217.97	23.08
12000	17.73	28.97	57.74	62.88	100.82	170.99	203.94	22.82
13000	17.70	28.95	58.04	63.15	101.14	165.35	191.65	22.58

Table 7.3 : Frequency dependence of real part of the permiability (μ') of Ni $_{1-x}$ Cd $_x$ Fe$_2$O$_4$ at the room temperature sintered at T$_s$=1150°C for 4 hours.

Frequency in kHz	x=0.0	x=0.1	x=0.2	x=0.3	x=0.4	x=0.5	x=0.6	x=0.8
1	17.28	35.77	52.67	86.10	134.34	258.69	492.59	50.63
2	17.28	35.77	52.67	86.10	134.34	258.69	482.54	50.63
3	17.28	35.77	52.67	86.10	134.34	258.69	482.54	50.63
4	17.28	35.77	52.67	86.10	134.34	258.69	482.54	50.63
5	17.28	35.77	52.67	86.10	134.34	258.69	472.49	50.63
6	17.28	35.77	52.67	86.10	134.34	258.69	472.49	50.63
7	19.87	37.56	51.61	82.27	136.26	256.01	472.49	47.59
8	19.87	37.56	51.61	82.27	136.26	256.01	471.48	47.59
9	19.87	37.56	51.61	82.27	136.26	256.01	470.48	47.59
10	19.87	37.56	51.61	82.27	136.26	256.01	469.47	46.58
20	19.87	36.67	51.61	81.32	135.30	254.23	465.45	46.58
30	19.87	36.67	51.61	81.32	135.30	254.23	463.44	46.58
40	19.87	36.67	51.61	81.32	135.30	253.33	461.43	46.58
50	19.87	36.67	51.61	81.32	135.30	253.33	460.42	46.58
60	19.87	36.67	51.61	81.32	135.30	252.44	459.42	46.58
70	19.87	36.85	51.09	81.22	135.02	252.44	458.61	46.27
80	19.87	36.85	50.98	81.22	134.92	252.26	457.61	46.17
90	19.87	36.76	50.98	81.12	134.92	252.00	457.21	46.17
100	19.79	36.76	50.98	81.12	134.82	251.73	456.80	46.07
200	19.79	36.76	50.88	80.93	134.54	250.30	450.07	45.77
300	19.79	36.67	50.77	80.93	134.34	249.14	444.64	45.46
400	19.79	36.67	50.77	80.84	133.38	248.25	440.42	45.16
500	19.70	36.67	50.67	80.74	134.06	247.54	436.30	44.96
600	19.70	36.58	50.56	80.65	133.96	246.82	434.29	44.75
700	19.61	36.56	50.56	80.58	133.86	246.38	431.07	44.64
800	19.61	36.52	50.51	80.53	133.83	245.93	428.25	44.48
900	19.53	36.49	50.47	80.47	133.78	245.66	425.04	44.33
1000	19.53	36.45	50.42	80.43	133.77	245.31	421.82	44.21
2000	19.28	36.21	50.09	80.16	134.06	242.63	381.91	42.94
3000	19.15	36.08	49.91	80.17	134.92	233.98	344.01	41.82
4000	19.06	35.99	49.81	80.36	135.49	220.86	313.55	40.71
5000	19.00	35.93	49.72	80.65	135.49	206.86	289.12	39.62
6000	18.96	35.86	49.72	80.93	135.02	193.75	269.52	38.58
7000	18.92	35.86	49.72	81.26	134.25	182.06	252.73	37.53
8000	18.89	35.84	49.73	81.65	133.19	171.71	238.76	36.59
9000	18.85	35.83	49.76	82.07	131.66	162.88	226.39	35.74
10000	18.84	35.83	49.82	82.49	129.93	155.29	215.53	34.98
11000	18.82	35.83	49.89	82.90	127.91	148.70	205.88	34.29
12000	18.79	35.45	49.96	83.27	125.61	142.90	197.14	33.67
13000	18.76	35.43	50.04	83.55	123.40	137.73	189.30	33.09

Table 7.4 : Frequency dependence of real part of the permiability (μ') of Ni $_{1-x}$ Cd $_x$ Fe$_2$O$_4$ at the room temperature sintered at T$_s$=1200°C for 4 hours.

Frequency in kHz	x=0.0	x=0.1	x=0.2	x=0.3	x=0.4	x=0.6	x=0.8
1	22.87	40.77	58.29	111.85	167.65	351.30	41.46
2	22.87	40.77	58.29	111.85	167.65	351.30	41.46
3	22.87	40.77	58.29	111.85	167.65	351.30	41.46
4	22.87	40.77	58.29	111.85	167.65	342.06	41.46
5	22.87	40.77	58.29	111.85	167.65	342.06	41.46
6	22.87	40.77	58.29	111.85	167.65	342.06	41.46
7	23.63	42.81	60.78	111.85	162.99	343.91	37.31
8	23.63	42.81	59.95	111.85	162.99	343.91	37.31
9	24.39	42.81	60.78	111.85	162.99	343.91	37.31
10	24.39	42.81	60.78	111.85	162.99	342.98	37.31
20	23.63	42.81	59.95	111.85	162.06	340.21	37.31
30	23.63	42.81	59.95	111.85	162.06	339.29	37.31
40	23.63	42.81	59.95	111.85	162.06	338.36	37.31
50	23.63	41.79	59.95	110.92	162.06	337.44	37.31
60	23.63	41.79	59.95	110.92	161.13	337.44	37.31
70	23.63	42.20	59.95	111.20	161.31	336.51	36.89
80	23.63	42.10	59.87	111.10	161.31	335.77	36.79
90	23.63	42.10	59.87	111.01	161.22	334.85	36.79
100	23.63	42.10	59.87	111.01	161.13	334.20	36.69
200	23.63	42.00	59.78	110.73	160.48	329.86	36.48
300	23.55	42.00	59.70	110.64	160.10	326.53	36.38
400	23.55	41.90	59.70	110.45	159.92	324.03	35.86
500	23.55	41.90	59.62	110.36	159.73	321.63	35.75
600	23.48	41.79	59.53	110.17	159.54	319.87	35.65
700	23.46	41.78	59.52	110.14	159.38	317.56	35.54
800	23.43	41.74	59.49	110.09	159.23	315.34	35.42
900	23.40	41.70	59.46	110.05	159.09	313.31	35.31
1000	23.38	41.65	59.44	110.02	158.98	311.18	35.20
2000	23.16	41.37	59.22	110.08	159.26	290.01	34.26
3000	23.05	41.19	59.20	111.10	159.64	270.04	33.49
4000	22.97	41.09	59.20	112.04	157.77	252.66	32.74
5000	22.92	41.03	59.37	112.04	153.49	237.69	32.09
6000	22.88	40.98	59.53	110.64	147.81	224.74	31.50
7000	22.84	40.97	59.75	108.26	141.60	213.19	30.96
8000	22.82	40.96	59.93	105.27	135.35	203.02	30.48
9000	22.80	40.95	60.10	102.02	129.40	193.96	30.05
10000	22.78	40.97	60.25	98.74	123.86	185.91	29.65
11000	22.76	41.00	60.38	95.55	118.82	178.61	29.29
12000	22.74	41.02	60.51	92.48	114.21	172.05	28.96
13000	22.71	41.03	60.56	89.58	110.05	166.22	28.62

Table 7.5 : Frequency dependence of real part of the permiability (μ') of Ni$_{1-x}$Cd$_x$Fe$_2$O$_4$ at the room temperature sintered at T$_s$=1250°C for 4 hours.

Frequency in kHz	x=0.0	x=0.1	x=0.2	x=0.3	x=0.4	x=0.5	x=0.6	x=0.8
1	31.53	47.89	94.43	120.39	177.81	216.06	342.00	41.46
2	31.53	47.89	94.43	120.39	177.81	216.06	331.64	41.46
3	31.53	47.89	94.43	120.39	177.81	216.06	331.64	41.46
4	31.53	47.89	94.43	120.39	177.81	216.06	331.64	41.46
5	31.53	47.89	94.43	120.39	177.81	216.06	331.64	41.46
6	31.53	47.89	94.43	120.39	177.81	216.06	331.64	41.46
7	27.59	46.93	93.38	121.40	173.86	215.03	330.60	41.46
8	27.59	46.93	92.33	121.40	173.86	214.00	330.60	41.46
9	27.59	46.93	92.33	121.40	173.86	214.00	329.57	41.46
10	27.59	46.93	92.33	121.40	173.86	214.00	330.60	41.46
20	27.59	46.93	92.33	121.40	172.87	212.97	327.49	41.46
30	26.80	46.93	92.33	121.40	172.87	211.95	326.46	41.46
40	26.80	46.93	92.33	120.39	171.89	211.95	325.42	40.42
50	26.80	46.93	92.33	120.39	171.89	211.95	324.39	40.42
60	26.80	46.93	92.33	120.39	171.89	210.92	323.35	40.42
70	26.56	46.64	91.81	120.50	171.20	210.92	323.35	40.42
80	26.56	46.74	91.70	120.50	171.49	210.92	322.62	40.52
90	26.56	46.64	91.60	120.39	171.29	210.92	322.21	40.42
100	26.56	46.64	91.60	120.39	171.10	209.89	321.48	40.42
200	26.56	46.64	91.28	119.99	170.50	209.06	316.30	40.11
300	26.56	46.54	91.18	119.79	169.91	208.04	312.99	39.90
400	26.48	46.54	90.97	119.59	169.61	207.21	309.88	39.69
500	26.48	46.45	90.86	119.49	169.32	206.39	307.39	39.49
600	26.48	46.45	90.76	119.29	169.12	205.77	305.21	39.38
700	26.44	46.42	90.71	119.17	168.44	205.36	303.14	39.25
800	26.41	46.38	90.63	119.11	168.39	204.64	301.27	39.11
900	26.39	46.34	90.57	119.07	168.30	204.13	299.31	38.99
1000	26.36	46.31	90.53	119.06	168.24	203.61	297.23	38.87
2000	26.18	46.09	90.53	119.49	168.73	199.70	272.36	37.87
3000	26.07	45.99	91.18	120.60	168.63	191.78	249.46	36.91
4000	25.99	45.95	92.02	120.90	164.68	181.59	230.90	35.95
5000	25.95	45.97	92.33	119.29	157.86	171.31	215.88	35.04
6000	25.91	45.97	91.60	115.88	149.66	161.74	203.44	34.19
7000	25.87	46.06	89.75	111.52	141.54	153.24	192.77	33.40
8000	25.84	46.14	87.22	106.94	133.86	145.83	183.57	32.71
9000	25.83	46.25	84.41	102.47	126.88	139.35	174.81	32.07
10000	25.81	46.38	81.56	98.31	120.65	133.64	167.63	31.50
11000	25.79	46.52	78.80	94.47	115.13	128.63	161.24	30.97
12000	25.77	46.65	76.19	90.95	110.23	124.05	155.46	30.48
13000	25.74	46.77	73.76	87.74	105.87	119.90	150.17	30.02

Table 7.6 : Temperature dependence permiability, μ' of Ni $_{1-x}$ Cd $_x$ Fe$_2$O$_4$. Curie temperature T_c is measured from $(dM/dT)_{max}$.

x=0.0		x=0.1		x=0.2		x=0.3	
Temp. (°C)	μ'	Temp. (°C)	μ'	Temp. (°C)	μ'	Temp. (°C)	μ'
30	107.16	30	151.64	30	136.39	30	231.71
50	107.78	50	152.46	50	138.05	78	251.66
70	107.78	70	152.86	70	139.72	130	274.03
90	108.40	90	154.29	90	141.55	170	279.62
110	107.94	130	155.92	130	145.38	210	291.74
150	107.78	150	156.33	150	147.21	220	293.6
170	107.94	170	158.37	170	148.71	230	295.47
200	108.55	190	159.18	190	150.38	240	296.4
220	108.40	210	159.79	210	151.38	250	295.47
240	108.40	230	160.2	230	152.71	260	295.93
260	108.40	250	161.02	250	153.04	270	295.93
280	108.24	270	162.04	270	153.54	280	295.47
300	108.24	290	162.24	290	153.87	290	295
320	108.24	310	162.44	310	154.21	300	293.6
340	107.94	320	162.24	330	152.38	310	291.74
380	108.09	330	162.44	350	151.54	315	291.27
400	107.94	340	162.44	370	150.21	320	290.34
420	108.40	370	161.63	390	149.04	330	288.94
440	108.40	380	161.83	395	148.38	340	286.15
460	108.71	390	161.22	400	148.21	345	285.21
480	109.32	400	160.81	405	147.55	350	285.21
500	109.63	420	160.41	410	147.55	355	285.68
520	110.25	430	160.2	415	147.21	360	286.61
540	110.87	440	160	420	147.38	365	288.01
560	111.80	450	159.79	430	147.71	370	289.88
580	113.03	460	159.59	435	147.88	374	279.16
588	113.80	480	159.59	440	148.21	375	272.63
589	113.96	490	159.59	445	148.88	376	250.26
590	113.96	500	159.79	450	149.38	377	237.68
595	113.23	510	159.39	455	151.54	378	232.09
596	112.72	520	159.59	460	153.21	379	224.16
597	112.41	530	159.59	465	149.88	380	214.38
598	112.26	540	159.39	466	148.71	381	205.99
599	111.80	545	159.39	467	146.21	382	203.38
600	111.02	550	159.59	468	145.38	383	195.92
601	110.41	555	159.59	469	142.38	384	191.26
602	110.25	560	166.52	470	139.72	386	181.75
605	108.24	565	165.3	480	130.23	387	178.4
610	102.38	570	163.87	490	123.90	389	173.37
615	98.05	575	162.65	505	118.07	390	168.52
620	97.28	580	160.81	525	113.57	400	151
625	97.28	585	159.18	545	111.41	420	135.52

Continuation of Table 7.6 .

x=0.4		x=0.5		x=0.6		x=0.8	
Temp. (°C)	μ'	Temp. (°C)	μ'	Temp. (°C)	μ'	Temp. (°C)	M (emu/g)
80	301.30	30	315.33	30	440.055	20	32.22
90	300.83	50	340.31	35	445.602	32	32.15
100	312.01	70	368.4	40	471.487	42	32.03
110	327.94	75	374.65	45	484.43	52	31.8
120	332.97	80	381.34	50	506.618	62	31.5
130	344.14	85	387.14	55	525.108	72	30.99
140	355.32	90	395.16	60	550.069	82	30.27
150	366.96	95	401.85	65	572.256	92	29.39
160	375.81	100	410.33	70	605.538	102	28.28
170	387.45	105	416.13	75	633.272	111	27.02
180	396.76	110	422.82	80	663.78	122	25.48
190	405.61	120	432.63	85	693.364	132	23.89
200	413.06	130	441.55	90	726.645	143	22.16
210	420.51	135	446.01	95	749.757	152	20.36
220	427.50	140	450.47	98	752.531	172	18.45
230	432.62	150	457.61	99	749.757	192	16.6
240	436.35	160	462.96	100	732.192	202	14.75
250	439.61	170	467.42	101	717.4	212	13.03
260	441.47	180	470.09	102	697.986	222	11.36
270	443.33	190	473.66	103	673.95	232	9.84
280	447.06	200	474.55	104	641.593	243	8.5
285	449.85	201	471.88	105	607.387	256	7.34
290	453.58	202	470.99	106	554.691	262	6.3
295	449.85	203	464.74	107	501.071	272	5.12
299	380.00	204	456.71	108	486.279	282	4.68
300	349.73	205	448.69	109	381.35	292	4.08
301	316.67	206	431.74	110	314.325	302	3.55
302	304.56	207	414.79	111	280.119	312	3.12
303	281.27	208	406.31	112	263.478	326	2.1
304	261.25	209	376.88	113	256.082	332	1.97
305	247.28	210	338.97	114	240.459	342	1.97
310	197.08	215	264.04	115	238.979		
315	180.31	220	225.68	116	231.584		
320	167.83	225	203.38	120	218.178		
325	160.75	230	185.9	125	210.783		
330	154.05	235	175.37	130	202.647		
345	144.92	240	164.49	135	200.798		

LIST OF THE IMPORTANT SYMBOLS AND UNITS USED

XRD	=	X-Ray Diffraction	$\tan \delta$	=	loss factor or loss tangent.
VSM	=	Vibrating Sample Magnetometer	δ	=	Phase difference
FWHM=		Full Width at Half Maximum	M_s	=	Saturation magnetization
T_m	=	Melting temperature	$H_{\hat{x}}, H_{\hat{y}}$	=	Stiffness in the x and y directions respectively.
T_c	=	Curie temperature			
K_1	=	Anisotropy constant	L	=	Self inductance of the sample core
H_c	=	Coercive force	L_o	=	Inductance of the winding coil without sample
μ	=	Permeability			
μ_m	=	Maximum permeability	[hkl]	=	Miller Indices
μ_i	=	Initial permeability	λ	=	Wave length of the X-ray
μ'	=	Real part of the complex permeability.	$\mu_i'/\tan\delta$	=	Relative quality factor
			T_s	=	Sintering temperature
μ''	=	imaginary part of the complex permeability.	A	=	Ampere
D	=	Grain size	emu	=	electromagnetic unit
H_z	=	Magnetic field in z-direction.	H	=	Henry
χ_r	=	Rotational susceptibility			
χ_w	=	wall susceptibility			
a_0	=	Lattice parameter			

Magnetic Term	Symbol	SI unit	CGS unit	Conversion factor
Magnetic induction	**B**	Tesla (T)	Gauss (G)	$1\ T = 10^4 G$
Magnetic field	**H**	A/m	Oersted (Oe)	$1\ A/m = 4\pi/10^3\ Oe$
Magnetization	**M**	A/m	emu/cm^3	$1\ A/m = 10^{-3}\ emu\ /cm^3$
Mass magnetization	σ	Am^2/kg	emu/g	$1\ Am^2/kg = 1\ emu/g$
Magnetic moment	**m**	Am^2	emu	$1\ Am^2 = 10^3\ emu$
Volume susceptibility	κ	dimensionless	dimensionless	4π (SI) = 1 (cgs)
Mass susceptibility	χ	m^3/kg	emu/Oe. g	$1\ m^3/kg = 10^3/4\pi\ emu\ /Oe.g$
Permeability of free space	μ_0	H/m	dimensionless	$4\pi \times 10^{-7}\ H/m = 1$ (cgs).